Highlighted paper selected by Editor-in-chief

Nicergoline Enhances Glutamate Uptake *via* Glutamate Transporters in Rat Cortical Synaptosomes

Atsushi NISHIDA,*[a] Hiroshi IWATA,[b] Yukitsuka KUDO,[c] Tsutomu KOBAYASHI,[a] Yuzo MATSUOKA,[a] Yoshikatsu KANAI,[d] and Hitoshi ENDOU[d]

[a] *Discovery and Pharmacology Research Laboratories, Tanabe Seiyaku Co., Ltd.; 2–2–50 Kawagishi, Toda, Saitama 335–8505, Japan:* [b] *Product Management Department, Pharmaceuticals Marketing Headquarters, Tanabe Seiyaku Co., Ltd.; 3–2–10 Dosho-machi, Chuo-ku, Osaka 541–8505, Japan:* [c] *Brain Function Research Institute, Inc., c/o National Cardiovascular Center; 5–7–1 Fujishiro-dai, Suita, Osaka 565–0873, Japan: and* [d] *Department of Pharmacology and Toxicology, Kyorin University School of Medicine; 6–20–2 Shinkawa, Mitaka, Tokyo 181–8611, Japan.*
Received November 28, 2003; accepted February 18, 2004

To elucidate the mechanisms of neuroprotective action of nicergoline, we examined its effect on glutamate transport in rat cortical synaptosomes and cloned glutamate transporters. In synaptosomes, nicergoline enhanced the glutamate uptake at 1—10 μM in standard medium and suppressed the increase of extracellular glutamate by reversed transport in low Na^+ medium. Apparent increase of extracellular glutamate concentration by dihydrokinate, an inhibitor of glial glutamate transporter GLT-1, was antagonized by nicergoline. In *Xenopus* oocytes expressing mouse neuronal glutamate transporter (mEAAC1), the glutamate-induced inward current was enhanced by nicergoline. These results suggest that nicergoline reduces the extracellular glutamate concentration through its effect on glutamate transporters.

Key words glutamate transporter; nicergoline; glutamate uptake; glutamate reversed transport; synaptosome; *Xenopus* oocyte

Glutamate transporters limit the extracellular concentration of glutamate ($[Glu]_o$) utilizing Na^+ electrochemical gradient as a driving force. Under physiological conditions, released glutamate in the synaptic cleft is transported into intracellular space by the glutamate transporters.[1—8] Substantial loss of glutamate uptake activity has been reported in some chronic neurodegenerative disorders including amyotrophic lateral sclerosis[9] and Alzheimer's disease.[10,11] When the intracellular Na^+ milieu is disturbed upon cerebral ischemia, the transporter functions in a reverse direction to release glutamate to neurotoxic levels.[1,12—14] Therefore, controlling the function of glutamate transporter is a potential therapeutic strategy for neuronal diseases.[15]

Nicergoline, a derivative of ergot alkaloid, is an ameliorator of cerebral circulation and metabolism.[16—24] In addition to enhancement of cholinergic[25—28] and dopaminergic transmissions in the brain,[29] protective actions of nicergoline against anoxic and/or ischemic brain damage and neuronal cell death are reported in several cerebral ischemic animals.[18—20,30] A recent study showed the neuroprotective action and the reduction of $[Glu]_o$ by nicergoline in ischemic rat brains.[31] Another ergort alkaloid, bromocriptine, was shown to enhance the glutamate transport activity.[11] In order to examine the effects of drugs on the uptake and reversed transport mediated by glutamate transporters, we previously developed an assay system in which extracellular glutamate concentration was measured in the synaptosome preparation.[32]

In the present study, in order to understand the mechanisms of action of nicergoline to reduce $[Glu]_o$, we examined its effect on the glutamate transport activity in rat cortical synaptosomes as well as on cloned glutamate transporters.

MATERIALS AND METHODS

Animals All experiments were performed in accordance with the regulations of the Animal Ethics Committee of TANABE Seiyaku Co., Ltd. Male Wistar strain rats weighing 200—400 g were used for preparation of crude synaptosomal fractions. *Xenopus laevis* (20—30 months old) were used for preparation of oocytes.

Synaptosomal Preparation Crude synaptosomal fractions were prepared following the standard procedures.[33] Rats were anesthetized with ether, and whole brains were removed after decapitation. The cerebral cortex, isolated under an ice-cold condition, was homogenized in a 5-fold volume of 0.32 M sucrose. The homogenate was centrifuged at $1500\times g$ for 10 min, and the supernatant was centrifuged at $9000\times g$ for 20 min. The pellet (P2 fraction) was suspended in 0.32 M sucrose solution again and centrifuged at $9000\times g$ for 20 min. The above procedures were carried out at 4 °C. The pellet was resuspended in 0.32 M sucrose, and used as a crude synaptosome preparation in the following experiments after determining the protein content. Protein content of the crude synaptosome preparation was 5.71 ± 0.18 mg/ml (mean±S.E., $n=15$). This preparation contained not only intra-synaptosomal glutamate, but also a small amount of extracellular glutamate. The glutamate in the synaptosomal preparation was of intrinsic origin.

Determination of Extracellular Glutamate in Synaptosomal Preparation Glutamate transporters mediate the uptake and the reversed transport of glutamate depending on both the electrochemical gradient of co-transported Na^+/counter-transported K^+ and the temperature.[34] Synaptosomes were incubated at 37 °C in standard HEPES buffered saline (HBS) medium containing 140.0 mM NaCl, 5 mM KCl, 5.0 mM $NaHCO_3$, 1 mM $MgCl_2$, 0.12 mM Na_2SO_4, 10 mM glucose, and 20 mM HEPES (pH 7.4). Fifty microliters of the crude synaptosome preparation was added to 1 ml of HBS or low Na^+ medium prepared by substituting Na^+ with choline. The synaptosomes in each medium with or without drugs were kept on ice until the start of the reaction. After incubation at 37 °C for up to 6 min, the transport reaction was terminated by immediately transferring the incubation tube into

* To whom correspondence should be addressed. e-mail: bon@tanabe.co.jp

an ice-cold water bath. Then, the synaptosomes were centrifuged at 9000×*g* for 20 min at 4 °C, and the supernatants were stocked at −80 °C until the measurement of glutamate contents. The concentration of glutamate in the supernatants was determined using the glutamate dehydrogenase-NADP method.[35]

***Xenopus* Oocytes** mRNA was *in vitro* transcribed from linearized pBluescript II SK (−) vector or pSP64poly(A) vector (Stratagene) containing the coding region of mEAAC1 (mouse EAAT-3) using T7 RNA polymerase (Stratagene). The *Xenopus laevis* oocytes were isolated by partial ovariectomy. After mild digestion with collagenase and defolliculation, oocytes were injected with cRNA solutions using a Drummond automatic injector Nanoject 203-VX (Drummond Scientific Company, U.S.A.). The injected volume was 50 nl/oocyte containing 30—80 ng of the cRNA. The oocytes were incubated at 18 °C in ND 96 solution (96 mM NaCl, 2 mM KCl, 1.8 mM $CaCl_2$, 1 mM $MgCl_2$, 5 mM HEPES, 2.5 mM Na-pyruvate, 0.5 mM theophylline, pH 7.5 with NaOH) containing penicillin (100 U/ml), streptomycin (100 μg/ml) and gentamicin (50 μg/ml).

Electrophysiology Two to 10 days after injection, oocytes were immersed in a normal external solution (NES) containing 96 mM NaCl, 2 mM KCl, 1.8 mM $CaCl_2$, 1 mM $MgCl_2$, and 5 mM HEPES, pH 7.5, and analyzed using the two-microelectrode voltage-clamp method at room temperature (22—23 °C). The microelectrodes were filled with a 3 M KCl solution, and their resistances were 0.5—2 MΩ. The membrane potential of an oocyte placed in a tissue chamber was clamped at −60 mV. Glutamate was applied to the bath, and the substrate-evoked inward current was recorded by a recording amplifier (GeneClamp 500, Axon Instruments Inc., U.S.A.). The effect of nicergoline was studied on the inward current induced by 10 μM glutamate in mEAAC1-expressing oocytes. The response of currents to a high concentration of glutamate (30 μM) was determined in each oocyte beforehand.

Chemicals The following materials were of reagent grade and obtained from commercial sources: HEPES (Nacalai Tesque Co., Ltd, Tokyo, Japan), glutamate dehydrogenase, NADP, collagenase, theophylline, penicillin, streptomycin, gentamicin (Sigma Chemicals Co., Ltd., St. Louis, MO, U.S.A.), dihydrokainic acid (DHK), bromocriptine (Tocris Cookson Inc., St. Louis, MO, U.S.A.). Nicergoline was provided by Pharmacia & Upjohn (Tokyo, Japan).

RESULTS

In synaptosome preparations, $[Glu]_o$ was reduced in standard HBS medium ($[Na^+]_o$=145.2 mM) and increased in low Na^+ medium by incubation for 6 min at 37 °C. The difference of the glutamate concentration before and after 37 °C incubation was expressed as $\Delta[Glu]_o$ (μM) {($[Glu]_o$ after incubation)−($[Glu]_o$ before incubation)}. "Positive" values of $\Delta[Glu]_o$ represent the increase whereas "negative" values represent the decrease of glutamate outside of synaptosomes. The $[Na^+]_o-\Delta[Glu]_o$ curve was shifted downwardly by nicergoline (Fig. 1). Namely, nicergoline enhanced the reduction of $[Glu]_o$ in standard HBS medium and reduced the elevation of $[Glu]_o$ in low Na^+ medium. However, the effect at the lowest Na^+ concentration ($[Na^+]_o$=5.24 mM) was not significant (Fig. 1).

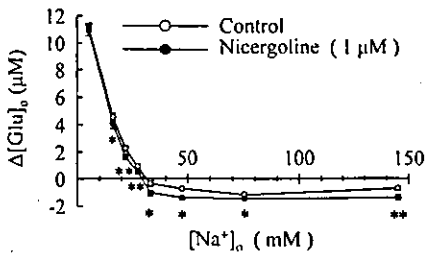

Fig. 1. Effects of Nicergoline on $[Na^+]_o-\Delta[Glu]_o$ Curve

Each point represents the mean±S.E. of 5 experiments. $*p<0.05$, $**p<0.01$ *vs.* control by paired *t*-test.

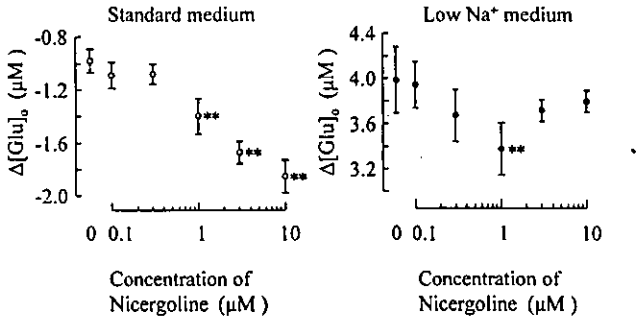

Fig. 2. Effects of Nicergoline on $\Delta[Glu]_o$ in Standard HBS Medium and Low Na^+ Medium

Low Na^+ medium was prepared by substitution of Na^+ with choline from 145.2 to 16.4 mM. Each point represents the mean±S.E. of 6 experiments. $**p<0.01$ *vs.* control, comparison by one-way ANOVA with randomized complete block, followed by multiple comparison (Tukey–Kramer's method).

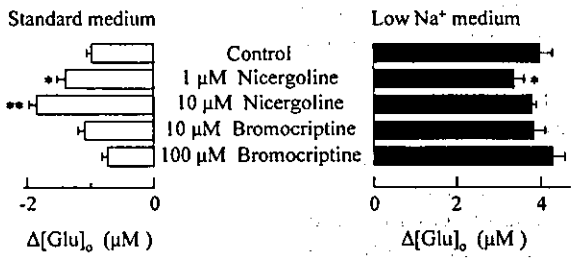

Fig. 3. Comparison of the Effects of Nicergoline and Bromocriptine on $\Delta[Glu]_o$

Low Na^+ medium was prepared by substitution of Na^+ with choline from 145.2 to 16.4 mM. Each column represents the mean±S.E. of 6 experiments. $*p<0.05$, $**p<0.01$ *vs.* control, comparison by one-way ANOVA with randomized complete block, followed by multiple comparison (Tukey–Kramer's method).

The reduction of $[Glu]_o$ by nicergoline in the standard HBS medium was concentration-dependent at doses between 1 and 10 μM. In contrast, the concentration–response relations in the low Na^+ medium ($[Na^+]_o$=16.4 mM) were statistically significant only at 1 μM, and formed a bell shaped curve (Fig. 2). In the same preparations, bromocriptine, an ergot alkaloid, had not effect $[Glu]_o$ (Fig. 3).

DHK, a selective inhibitor of glial glutamate transporter GLT-1,[32,33] suppressed the reduction of $[Glu]_o$ in a standard HBS medium and enhanced the elevation of $[Glu]_o$ in low Na^+ medium ($[Na^+]_o$=16.4 mM). Nicergoline at 1 μM antagonized both effects of DHK (Fig. 4).

In oocytes expressing mEAAC1, inward current was evoked by perfusion of glutamate in the recording chamber.

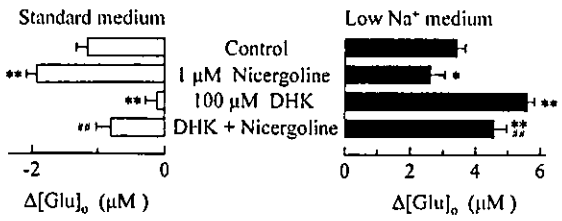

Fig. 4. Effects of Nicergoline and DHK on $\Delta[Glu]_o$

Low Na^+ medium was prepared by substitution of Na^+ with choline from 145.2 to 16.4 mM. Each column represents the mean±S.E. of 4 experiments. $*p<0.05$, $**p<0.01$ *vs.* control, $\#p<0.01$ *vs.* DHK-treatment, comparison by one-way ANOVA with randomized complete block, followed by multiple comparison (Tukey–Kramer's method).

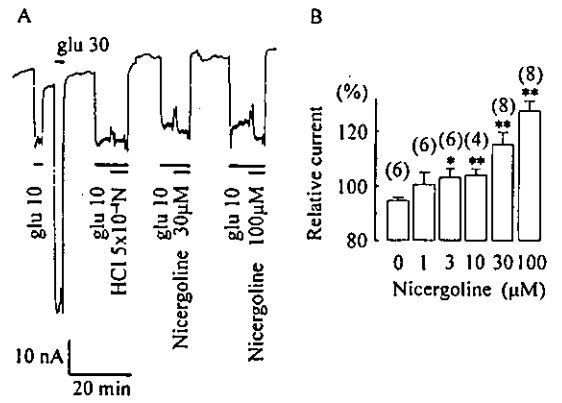

Fig. 5. Effects of Nicergoline on the Inward Currents Induced by 10 μM Glutamate in *Xenopus* Oocytes Expressed EAAC1

(A) Typical current trace recorded from an EAAC1-expressing oocyte at a holding potential of −60 mV in the presence of various concentrations of nicergoline. The ratio of effects by vehicle, 30 μM and 100 μM nicergoline were 98.0%, 109.9% and 124.2%, respectively. (B) The current after application of nicergoline is expressed relative to the current evoked by glutamate alone. For a concentration of 0 μM, only the vehicle (5×10^{-4} N HCl) was applied. Each column represents the mean±S.E. of the numbers indicated in parentheses. $*p<0.05$, $**p<0.01$ *vs.* control by Student's *t*-test. The solvent (HCl 5×10^{-4} N) only slightly reduced the inward current. Nicergoline significantly increased the glutamate-induced inward current in a concentration-dependent manner (Fig. 5).

DISCUSSION

Incubating a synaptosome preparation at 37 °C decreased or increased the $[Glu]_o$ depending on the concentration of Na^+ in the medium. $\Delta[Glu]_o$ is reversed from negative to positive values when the extracellular Na^+ concentration is decreased to ~30 mM.[32] Because these processes are highly sensitive to temperature but not dependent on Ca^{2+}, it is proposed that the reduction and the elevation mainly reflect the uptake into and reversed transport from synaptosomes, respectively. The uptake of glutamate by the transporters requires sufficient concentration of Na^+, whereas the reversed transport becomes dominant in low Na^+ medium. The direction and the magnitude of $\Delta[Glu]_o$ appeared to be determined by a balance of the uptake and reversed transport. $\Delta[Glu]_o$ was reduced by nicergoline under both standard and low Na^+ conditions.

Both neuronal and glial transporters participate in the control of extracellular glutamate concentration. $[Glu]_o$ was decreased due to the uptake by both transporters in the standard HBS medium. Because the intracellular concentration of glutamate is high (1 mM) in neurons, neuronal glutamate transporters are assumed to function in the reverse direction before glial transporters do when Na^+ homeostasis is disrupted in brain ischemia or under anoxic conditions. DHK, a selective inhibitor of glial GLT-1 glutamate transporter,[36,37] suppressed the decrease of $[Glu]_o$ in standard HBS medium and enhanced the elevation of $[Glu]_o$ in low Na^+ medium.[32] The increase of $\Delta[Glu]_o$ by DHK in low Na^+ medium indicates the existence of uptake *via* glial glutamate transporter GLT-1 even under the low Na^+ condition.

The DHK-induced increase of $[Glu]_o$ is suppressed by nicergoline in both standard HBS and low Na^+ media. Glutamate transporters work mainly in the forward direction (uptake) in the standard HBS medium and in the reverse direction in the low Na^+ medium. The concentration-dependent effect of nicergoline was more pronounced in standard HBS medium than in low Na^+ medium. However, there was no reduction of $\Delta[Glu]_o$ by nicergoline at the lowest Na^+ concentration. When Na^+ concentration is 5.24 mM GLT-1 does not uptake extracellular glutamate. Thus, nicergoline reduces $[Glu]_o$ by enhancing the uptake rather than inhibiting the reversed transport of glutamate.

Bromocriptine was reported to enhance the uptake of glutamate by human GluT-1[15,38] stably expressed in HeLaS3 cells. GluT-1 is a subtype of glutamate transporters expressed predominantly in cerebellum[39] among brain regions. We used synaptosome from rat cerebral cortex without cerebellum. In this study, bromocriptine failed to enhance the uptake of glutamate; this lack of effect may have been due to low abundance of GluT-1 in the preparation.

In order to further confirm the effect of nicergoline on glutamate transporters, we determined the effect on cloned neuronal transporter EAAC1. We used mouse EAAC1 that was 97% homologous at the amino acid level with rat EAAC1. Nicergoline increased the glutamate-induced current mediated by EAAC1. Although we also attempted to examine the effect of nicergoline on cloned glial transporter encoded by GLT-1, the glutamate-induced current mediated by GLT-1 was too small to make this evaluation. It has been reported that glutamate transporter is regulated by transporter-associated proteins.[40] Thus, inhibition of the function of the associating protein may result in the enhancement of the glutamate transport. Although the mechanisms behind the action of nicergoline remain unclear at this moment, it is possible that nicergoline acts on the transporter-associated protein to enhance the transport function.

In this study, we showed the enhancement of neuronal glutamate transport by nicergoline in both oocytes expressing mEAAC1 and synaptosomes in the presence of DHK. Although the function of EAAC1 was changed from uptake to reversed transport in lower Na^+ condition, the uptake was enhanced by nicergoline except for the lowest Na^+ concentration. Therefore, we propose that nicergoline acts on both glial and neuronal glutamate transporters.

Extracellular concentration of glutamate is crucial for the development of neuronal damage following ischemia.[1,12–14] Enhancement of glutamate uptake by nicergoline may, at least in part, contribute to the reduction of glutamate concentration in the brain which results in ischemia. The synaptosome prepared from rat cerebral cortex includes at least two subtypes of glutamate transporters, EAAC1 and GLT-1. Human EAAC1 and human GLT-1 are 90% and 91% homologous at the amino acid level with rat EAAC1 and rat GLT-1, respectively. Thus it is reasonable to speculate that a similar

effect of nicergoline can be expected in both rodents and humans.

The concentration of nicergoline in the central nervous system at a clinical dosage (15 mg/day) is expected to reach sub microM order, which is comparable to the effective concentration in the present study. Nicergoline reduces $[Glu]_o$ in the brain and protects brain damage by ischemia in rats.[31] Thus, the demonstration of transporter-modulating activity warrants consideration of a clinical neuroprotective effect of nicergoline.

Acknowledgments We thank Professor Shigenobu Nakamura and Dr. Hideshi Kawakami, Hiroshima University, for their valuable advice on this work. We also thank Dr. Akira Saito for valuable discussions during the preparation of this article.

REFERENCES

1) Bouvier M., Szatkowski M., Amato A., Attwell D., *Nature* (London), **360**, 471—474 (1992).
2) Kanai Y., Hediger M. A., *Nature* (London), **360**, 467—471 (1992).
3) Kanai Y., Smith C. P., Hediger M. A., *Trends Neurosci.*, **16**, 365—370 (1993).
4) Kawakami H., Tanaka K., Nakayama T., Inoue K., Nakamura S., *Biochem. Biophys. Res. Commun.*, **199**, 171—176 (1994).
5) Pines G., Danbolt N. C., Bjoras M., Zhang Y., Bendahan A., Eide L., Koepsell H., Storm-Mathisen J., Seeberg E., Kanner B. I., *Nature* (London), **360**, 464—467 (1992).
6) Robinson M. B., Hunter-Ensor M., Sinor J., *Brain Res.*, **544**, 196—202 (1991).
7) Tanaka K., *Neurosci. Res.*, **16**, 149—153 (1993).
8) Tanaka K., *Neurosci. Lett.*, **159**, 183—186 (1993).
9) Rothstein J. D., Martin L. J., Kuncl R. W., *New Engl. J. Med.*, **326**, 1464—1468 (1992).
10) Li S., Mallory M., Alford M., Tanaka S., Masliah E., *J. Neuropathol. Exp. Neurol.*, **56**, 901—911 (1997).
11) Palmer A. M., Proctor A. W., Stratmann G. C., Bowen D. M., *Neurosci. Lett.*, **66**, 199—204 (1986).
12) Attwell D., Barbour B., Szatkowski M., *Neuron*, **11**, 401—407 (1993).
13) Kanai Y., Stelzner M., Nussberger S., Khawaja S., Hebert S. C., Smith C. P., Hediger M. A., *J. Biol. Chem.*, **269**, 20599—20606 (1994).
14) Levi G., Raiteri M., *Trends Neurosci.*, **16**, 415—419 (1993).
15) Yamashita H., Kawakami H., Zhang Y., Tanaka K., Nakamura S., *Lancet*, **346**, 1305 (1995).
16) Heitz C., Descombes J. J., Miller R. C., Stoclet J. C., *Eur. J. Pharmacol.*, **123**, 279—285 (1986).
17) Iwata E., Miyazaki I., Asanuma M., Iida A., Ogawa N., *Neurosci. Lett.*, **251**, 49—52 (1998).
18) LePoncin-Lafitte M., Grosdemouge C., Duterte D., Rapin J. R., *Gerontology*, **30**, 109—119 (1984).
19) Shintomi K., Egou H., Tanaka T., Itakura T., Yoshimoto K., Matsumoto M., Matsuoka Y., *Folia Pharmacol. Japon*, **87**, 445—456 (1986).
20) Shintomi K., Itakura T., Yoshimoto K., Ogawa Y., Fukushima T., Matsuoka Y., *Folia Pharmacol. Japon*, **87**, 427—434 (1986).
21) Shintomi K., Ogawa Y., Yoshimoto K., Narita H., *Folia Pharmacol. Japon*, **87**, 537—549 (1986).
22) Shintomi K., *Arzheim.-Forsch. Drug Res.*, **41**, 885—890 (1991).
23) Takahashi K., Akaike N., *Br. J. Pharmacol.*, **100**, 705—710 (1990).
24) Tanaka M., Yoshida T., Okamoto K., Hirai S., *Neurosci. Lett.*, **248**, 68—72 (1998).
25) Carfagna N., Diclemente A., Cavanus S., Damiani D., Gerna M., Salmoiraghi P., Cattaneo B., Post C., *Neurosci. Lett.*, **197**, 195—198 (1995).
26) Kudo Y., Egou H., Ishida R., *Jpn. Pharmacol. Ther.*, **13**, 6489—6493 (1985).
27) Ogawa N., Mizukawa K., Haba K., Asanuma M., *Geriat. Med.*, **27**, 1198—1204 (1989).
28) Ogawa N., Asanuma M., Hirata H., Kondo Y., Kawada Y., Mori A., *Arch. Geront. Geriatr.*, **16**, 103—110 (1993).
29) Moretti A., Carfagna N., Caccia C., Carpentieri M., *Arch. Int. Pharmacodyn. Ther.*, **294**, 33—45 (1988).
30) Iwasaki H., *Jpn. Pharmacol. Ther.*, **18**, 1995—2004 (1990).
31) Asai S., Zhao H., Yamashita A., Jike T., Kunimatsu T., Nagata T., Kohno T., Ishikawa K., *Eur. J. Pharmacol.*, **383**, 267—274 (1999).
32) Nishida A., Kobayashi T., Kudo Y., Matsuoka Y., *Jpn. J. Pharmacol.* (Suppl. 1), **76**, 85P (1998).
33) Hajos F., *Brain Res.*, **93**, 485—489 (1975).
34) Allen J. W., Shanker G., Aschner M., *Brain Res.*, **894**, 131—140 (2001).
35) Graham L. T., Jr., Aprison M. H., *Anal. Biochem.*, **15**, 487—497 (1966).
36) Chatton J. Y., Shimamoto K., Magistretti P. J., *Brain Res.*, **893**, 46—52 (2001).
37) Kanai Y., *Curr. Opin. Cell Biol.*, **9**, 565—572 (1997).
38) Yamashita H., Kawakami H., Zhang Y. X., Tanaka K., Nakamura S., *J. Neurol. Sci.*, **155**, 31—36 (1998).
39) Nakayama T., Kawakami H., Tanaka K., Nakamura S., *Brain Res. Mol. Brain Res.*, **36**, 189—192 (1996).
40) Lin C. I., Orlov I., Ruggiero A. M., Dykes-Hoberg M., Lee A., Jackson M., Rothstein J. D., *Nature* (Londond), **410**, 84—88 (2001).

Lysophosphatidylcholine Enhances Cytokine Production of Endothelial Cells via Induction of L-Type Amino Acid Transporter 1 and Cell Surface Antigen 4F2

Wakako Takabe, Yoshikatsu Kanai, Arthit Chairoungdua, Noriyuki Shibata, Sono Toi, Makio Kobayashi, Tatsuhiko Kodama, Noriko Noguchi

Objective—A diverse range of lipid oxidation products detected in oxidized low-density lipoprotein (oxLDL) and atherosclerotic lesions are capable of eliciting biological responses in vascular cells. We performed DNA microarray experiments to explore novel responses of human umbilical vein endothelial cells (HUVECs) to oxLDL and its components.

Methods and Results—cDNA microarray analysis showed that oxLDL, lysophosphatidylcholine (LysoPC), 4-hydroxy-2-nonenal, and oxysterols altered gene expression specifically, but some genes were commonly induced in HUVECs. Solute carrier family 3 member 2 and family 7 member 5, encoding the heavy chain of the cell surface antigen 4F2 (4F2hc) and the L-type amino acid transporter 1 (LAT1), respectively, were induced by oxLDL and many oxidation products. LAT1 requires 4F2hc to form a heterodimeric functional complex to transport neutral amino acids into the cell. LysoPC increased membrane protein levels of LAT1 confirmed by Western blot analysis and also uptake of L-[^{14}C]leucine, which was inhibited by a competitive inhibitor for LAT1. The release of interleukin 6 (IL-6) and IL-8 was increased in LysoPC-treated cells and was attenuated by the LAT1 inhibitor.

Conclusions—These findings suggest that an increase in uptake of neutral amino acids induced by LysoPC results in enhancement of inflammatory responses of endothelial cells. (***Arterioscler Thromb Vasc Biol.* 2004;24:1640-1645.**)

Key Words: amino acid transporter ■ atherosclerosis ■ cytokine ■ HUVEC ■ LysoPC

Atherosclerosis, which leads to coronary heart disease and stroke, is the most common cause of death in industrialized nations. It has been suggested that oxidative modification of low-density lipoprotein (LDL) is a key initial event in atherosclerosis pathogenesis,[1] and a wide variety of oxidized lipids have been detected in atherosclerotic lesions.[2] LDL is composed of a cholesteryl ester (CE) and triglyceride core with an outer monolayer composed of phosphatidylcholine (PC) and free cholesterol solubilized in blood by 1 molecule of apolipoprotein.[3] The esterified fatty acids of PC and CE are oxidized enzymatically and nonenzymatically to yield lipid hydroperoxides as the primary products,[4] followed by secondary reactions to form lipid hydroxides and aldehydes such as malondialdehyde, acrolein,[5] and 4-hydroxy-2-nonenal (4HNE). Acrolein and 4HNE are known to be highly reactive and to form adducts with proteins and nucleic acids.[6] In particular, many studies have shown that 4HNE regulates cell-signaling pathways through activation protein 1 (AP-1).[7–9] Cholesterol is also oxidized to give several classes of oxysterols: 7-ketocholesterol, which induces monocyte differentiation and promotes foam cell formation;[10] 22(*R*)-hydroxycholesterol, which is a ligand for the liver X receptor and regulates the expression of genes involved in cholesterol and fatty acid homeostasis;[11] and 25-hydroxycholesterol, which regulates cholesterol synthesis via the sterol regulatory element-binding protein (SREBP)/SREBP cleavage–activating protein regulatory pathway.[12] Lysophosphatidylcholine (LysoPC) is present at high concentrations in oxidized LDL (oxLDL) and formed via the reaction of phospholipase A2. α-Palmitoyl-LysoPC (16:0) is known to induce various protein kinases in vascular cells, including protein kinase C (PKC), extracellular signal regulated kinase (ERK) 1 and 2 (ERK1/2), and p38.[13–16]

We performed large-scale gene expression analysis using human endothelial cells exposed to oxLDL and lipid oxidation products such as LysoPC, 4HNE, 7-ketocholesterol, 22(*R*)-hydroxycholesterol, and 25-hydroxycholesterol contained in oxLDL. There were several genes that were commonly induced by oxLDL and some of the oxidation products, but they were assumed to be important from the

Received April 19, 2004; revision accepted May 17, 2004.

From the Laboratory for Systems Biology and Medicine (W.T., T.K., N.N.), Research Center for Advanced Science and Technology, The University of Tokyo, Japan; Chugai Pharmaceutical Co Ltd (W.T.), Shizuoka, Japan; the Department of Pharmacology and Toxicology (Y.K., A.C.), Kyorin University School of Medicine, Tokyo, Japan; and the Departments of Pathology (N.S., M.K.) and Neurology (S.T.), Tokyo Women's Medical University, Tokyo, Japan.

Correspondence to Noriko Noguchi, Laboratory for Systems Biology and Medicine, Research Center for Advanced Science and Technology, The University of Tokyo, 4-6-1 Komaba, Meguro, Tokyo, 153-8904, Japan. E-mail noguchi@lsbm.org

Arterioscler Thromb Vasc Biol. is available at http://www.atvbaha.org DOI: 10.1161/01.ATV.0000134377.17680.26

Upregulated Genes by oxLDL and its Components

Gene Name	Description of Protein	GenBank Accession No.	Fold Change (Mean±SD)					
			oxLDL	LysoPC	4HNE	7keto	22(R)OH	25OH
HMOX1	heme oxygenase (decycling) 1	Z82244	39.09±8.49	2.75±1.41	19.8±10	1.08±0.19	1.3±0.22	1.11±0.18
ATF3	activating transcription factor 3	AB066566	6.57±2.86	2.03±0.98	1.15±0.08	1.13±0.5	0.96±0.39	0.92±0.28
CEBPB	CCAAT/enhancer-binding protein (C/EBP), beta	X52560	4.3±3.71	6.59±2.54	2.5±1.43	1.27±0.53	2.16±0.3	1.64±0.71
VEGF	vascular endothelial growth factor	AF437895	3.32±3.6	6.03±6.84	0.99±0.17	1.17±0.61	1.52±0.54	0.94±0.51
PMAIP1	phorbol-12-myristate-13-acetate-induced protein 1	BC013120	3.29±1.73	3.72±2.83	0.95±0.34	1.35±0.37	1.39±0.55	1.17±0.65
SLC3A2	solute carrier family 3, member 2	AB018010	2.89±0.75	1.97±0.29	2.79±0.48	1.33±0.25	2.42±0.36	1.4±0.3
PTGS2	cyclooxygenase 2	AF044206	2.82±0.95	17.35±7.54	9.99±7.77	1.32±0.54	1.05±0.16	2.03±1.07
SLC7A5	solute carrier family 7, member 5	AB017908	2.41±1.63	4.58±2.1	1.86±0.92	1.46±0.48	1.95±0.47	1.51±0.55
DUSP1	dual specificity phosphatase 1	U01669	2.1±0.22	5.56±2.88	1.62±0.38	1.1±0.09	1.25±0.26	1.18±0.05
ADAMTS1	a disintegrin-like and metalloprotease type 1 motif, 1	AP001697	2.03±0.42	15.8±16.36	0.62±0.13	1.11±0.68	0.79±0.19	1.33±0.84

HUVEC were treated with oxLDL (200 μg/mL), LysoPC (30 μmol/L), 4HNE (5 μmol/L), 22- hydroxycholesterol (22(R)OH, 10 μmol/L), 25- hydroxycholesterol (25OH, 10 μmol/L), and 7-ketocholesterol (7keto, 10 μmol/L) for 4 hours. The numbers of fold change are shown as mean±SD of three independent experiments.

therapeutic point of view. In this article, we report the induction of solute carrier genes that encode for an amino acid transporter subfamily.

Amino acid transporters in the plasma membrane mediate the uptake of nutrients into cells. Among the documented amino acid transport systems, system L is a major transport system for the Na^+-independent nutrient uptakes, whereas 2-aminobicyclo-(2,2,1)-heptane-2-carboxylic acid (BCH) is involved in the sensitive transport of large neutral amino acids.[17]

The L-type amino acid transporter 1 (LAT1) belongs to system L and requires the heavy chain of the cell surface antigen 4F2 (4F2hc) for functional expression. It transports neutral amino acids, most of which are essential amino acids.[18–20] Although the expression of 4F2hc is apparently ubiquitous, LAT1 is expressed in the brain, placenta, testes, bone marrow, fetal liver, and peripheral leukocytes.[18,21] Furthermore, LAT1 is highly expressed in certain tumor cell lines[18] as well as in malignant tumors.[22] Because overexpression of LAT1 supports the high protein synthesis rates in growing cells, this finding has given rise to the suggestion that LAT1 might be a useful therapeutic target. The consequence of the increased protein synthesis in endothelial cells should be another important issue to be investigated. This article reports for this first time that increased LAT1 expression can be induced by lipid oxidation products relevant to inflammatory responses in atherogenesis.

Methods

Cell Culture and Treatment

Human umbilical vein endothelial cells (HUVECs) and human aortic endothelial cells (HAECs) were obtained from a commercial source (Clonetics, San Diego), and all experiments were conducted in 4 passages. HUVECs and HAECs were grown in endothelial cell growth factor–containing medium-2 (EGM-2; Clonetics) with 2% FBS (Clonetics) at 37°C in a 5% CO_2 atmosphere. After reaching confluence, the medium was changed to EGM-2 with 2% FBS containing 200 μg/mL oxLDL, 10 μmol/L 7-ketocholesterol (Steraloids Inc), 10 μmol/L 22(*R*)-hydroxycholesterol (Sigma), 10 μmol/L 25-hydroxycholesterol (Sigma), 30 μmol/L α-palmitoyl-LysoPC (Sigma), or 5 μmol/L 4HNE (Cayman Chemical). All chemicals were dissolved in ethanol (EtOH; Wako), which was diluted with EGM-2, resulting in a final EtOH concentration of 0.01%. The control cells were cultured in EGM-2 containing 0.01% EtOH in the absence of oxidation products.

Details for methods of measurement of lipid oxidation products in oxLDL, Northern blot and real-time polymerase chain reaction (PCR) analysis, Western blot analysis, L-leucine uptake, measurement of cytokines, immunohistochemical study, adhesion molecule measurement, and others are in the expanded Methods section available online at http://atvb.ahajournal.org.

Results

Effect of oxLDL and Its Components on Gene Expression in HUVECs

In preliminary experiments, concentrations of lipid oxidation products were first assessed from samples of oxLDL (200 μg/mL) oxidized for 18 hours with 100 μmol/L copper. This treatment results in extensively oxidized LDL and allows for a feasible assessment of the maximum concentrations of individual components likely to stimulate a biological response. No toxicity was evident under any conditions for 24 hours as assessed by crystal violet staining and trypan blue exclusion method (data not shown).

Gene expression was determined in HUVECs using the GeneChip human genome focus array, which contains 8794 genes. Expression was determined in response to 200 μg/mL oxLDL, 10 μmol/L 7-ketocholesterol, 10 μmol/L 22(*R*)-hydroxycholesterol, 10 μmol/L 25-hydroxycholesterol, 30 μmol/L LysoPC, and 5 μmol/L 4HNE. The concentration of each oxidation product was determined according to that of oxLDL used in the present study.

Whereas oxLDL, LysoPC, and 4HNE induced expression of 117 genes, 105 genes, and 14 genes, respectively, a few genes were responsive to 3 different kinds of oxysterols: 0 7-ketocholesterol, 5 22(*R*)-hydroxycholesterol, and 1 25-hydroxycholesterol, respectively. The table shows the genes that were upregulated by 4 hours of treatment with oxLDL >2-fold. The fold change values obtained by treatment with oxidation products are also shown. Among these upregulated genes, the solute carrier family (SCL) genes were induced not only by oxLDL but also LysoPC, 4HNE, and 22(*R*)-hydroxycholesterol. SCL genes are known to encode transporter subunits. Another interesting gene induced by oxLDL,

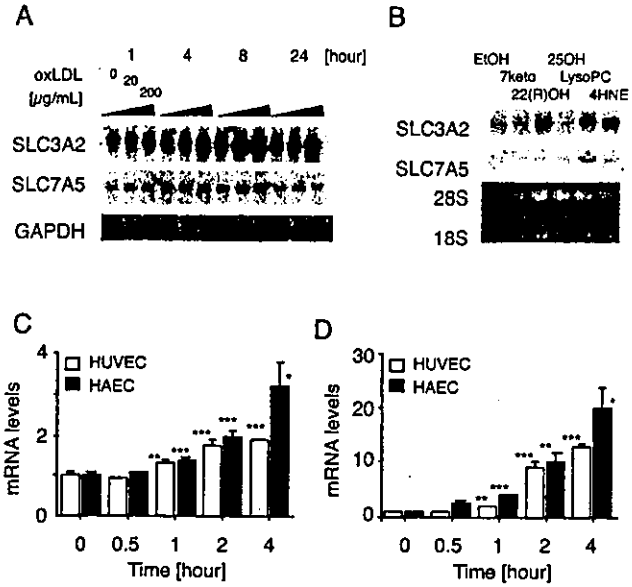

Figure 1. Time- and concentration-dependent induction of mRNA expression of *SLC3A2* and *SLC7A5* by oxLDL and its components. A, Northern blot analysis was used to determine treatment effect of HUVECs with 20 or 200 μg/mL oxLDL for up to 24 hours on mRNA expression levels of *SLC3A2* and *SLC7A5*. B, Induction of *SLC3A2* and *SLC7A5* by oxidized LDL components in HUVECs was examined. HUVECs were treated by 10 μmol/L 7-ketocholesterol (7keto), 10 μmol/L 22(*R*)-hydroxycholesterol (22(*R*)OH), 10 μmol/L 25-hydroxycholesterol (25OH), 30 μmol/L LysoPC, or 5 μmol/L 4HNE for 4 hours. All chemicals were dissolved in EtOH. 28.5 and 18.5 indicate ribosomal RNA. Real-time PCR analysis were performed for *SLC3A2* (C) and *SLC7A5* (D) expression induced by LysoPC in HUVECs and HAECs. All data obtained were normalized by GAPDH values and shown as the mean±SD (n=3) of the ratio against time 0. *$P<0.05$; **$P<0.01$; ***$P<0.005$.

LysoPC, 4HNE, and 22(*R*)-hydroxycholesterol was the CCAAT/enhancer-binding protein β (C/EBPβ), a nuclear factor for interleukin 6 (IL-6) and IL-8 expression.

Induction of mRNA of *SLC3A2* and *SLC7A5* by oxLDL

In the next series of experiments, we verified the accuracy of the GeneChip findings by Northern blot analysis for *SLC3A2* and *SLC7A5*. HUVECs were exposed to extensively oxidized LDL (20 or 200 μg/mL) for up to 24 hours. Figure 1A shows that oxLDL induced the expression of both *SLC3A2* and *SLC7A5* in a time- and concentration-dependent manner for up to 8 hours. The concentration of LysoPC in this oxLDL was measured and found to be 66.8 (mol/mol LDL). Thus, the concentration of LysoPC in medium was ≈30 μmol/L when 200 μg/mL oxLDL was added into medium. We measured other oxidation products in this oxLDL and calculated the concentration of each of them in medium as follows: 4.4 μmol/L 7-ketocholesterol, 2.7 μmol/L 22(*R*)-hydroxycholesterol, 5.4 μmol/L 25-hydroxycholesterol, and 0.5 μmol/L 4HNE.

Induction of mRNA of *SLC3A2* and *SLC7A5* by oxLDL Components

HUVECs were treated with 10 μmol/L 7-ketocholesterol, 10 μmol/L 22(*R*)-hydroxycholesterol, 10 μmol/L 25-hydroxycholesterol, 30 μmol/L LysoPC, and 5 μmol/L 4HNE. The microarray data showed that the fold change of *SLC3A2* induced by LysoPC, 4HNE, or 22(*R*)-hydroxycholesterol was 1.97±0.29, 2.79±0.48, and 2.42±0.36, respectively, and that of *SLC7A5* by LysoPC, 4HNE, or 22(*R*)-hydroxycholesterol was 4.58±2.10, 1.86±0.92, and 1.95±0.47, respectively. These results agree with the results of the Northern blot analysis (Figure 1B).

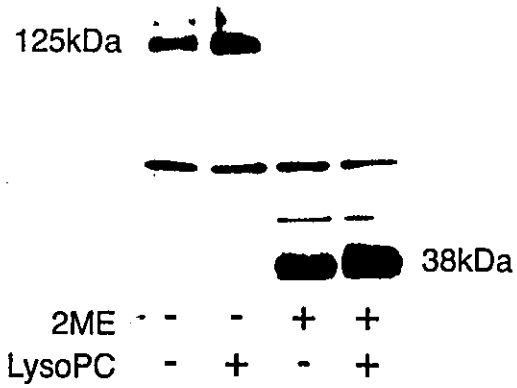

Figure 2. Increase in protein levels of LAT1 induced by LysoPC. Western blot analysis using a monoclonal antibody against LAT1 was performed for the membrane fraction (5 μg of protein) prepared from HUVECs after treatment with or without 30 μmol/L LysoPC for 6 hours. The 125-kDa protein band detected in the nonreducing condition shifted to a 38-kDa protein band by the treatment of 2-mercaptoethanol (2ME).

Because LysoPC is one of the most abundant oxidation products in oxLDL and induced SLC genes most extensively, the time-dependent induction of mRNA of *SLC3A2* and *SLC7A5* in HUVECs treated with 30 μmol/L LysoPC was followed for up to 4 hours by quantitative real-time PCR (Figure 1C and 1D). All data normalized by GAPDH and cyclophilin showed almost the same results. The expression of *SLC3A2* and *SLC7A5* was increased over time. The same experiments were performed for HAECs and showed that LysoPC induced mRNA both of *SLC3A2* and *SLC7A5* in aortic endothelial cells in a time-dependent manner.

Induction of Amino Acid Transporter Protein by LysoPC

We confirmed an increase in LAT1 (*SLC7A5*) protein level in membrane fraction of HUVECs after exposure to 30 μmol/L LysoPC for 6 hours (Figure 2). The 125-kDa protein corresponding to a heterodimeric complex of LAT1 and 4F2hc was detected under the nonreducing condition. The band of 38-kDa protein corresponding to LAT1 monomer appeared by reducing the protein complex with 2-mercaptoethanol.

Effect of LysoPC on L-[^{14}C]Leucine Uptake in HUVECs

The effect of LysoPC on amino acid transport in HUVECs was examined using L-[^{14}C]leucine (Figure 3). LysoPC increased L-[^{14}C]leucine uptake significantly after 6 hours of incubation, the effect of which was almost completely inhibited by 1 mmol/L BCH, a selective inhibitor of system L amino acid transporter (LAT1, LAT2, and LAT3) under Na^+-free conditions. The GeneChip data showed that *SLC7A8* encoding LAT2 was not expressed in HUVECs and

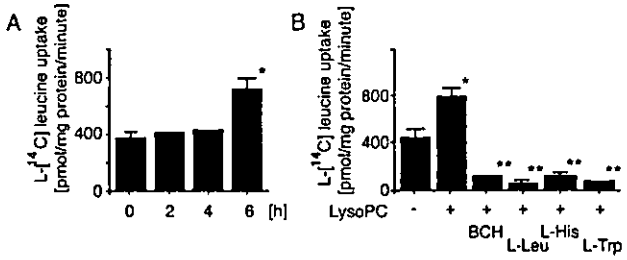

Figure 3. The effect of LysoPC on L-[^{14}C]leucine uptake in HUVECs. Induction of L-[^{14}C]leucine transport in HUVECs treated with 30 μmol/L LysoPC for 6 hours (A). HUVECs were incubated in the Na^+-free uptake solution containing 10 μmol/L L-[^{14}C]leucine for 1 minute, and the L-[^{14}C]leucine uptake was measured in the presence or absence of 1 mmol/L BCH, 1 mmol/L L-leucine (L-Leu), 1 mmol/L L-histidine (L-His), and 1 mmol/L L-tryptophan (L-Trp) (B). Each was performed in triplicate. *P<0.05 vs no addition and **P<0.005 vs LysoPC.

also was not induced by LysoPC (1.30±0.30). *SLC43A1* (named prostate cancer overexpressed gene 1) encoding LAT3 was expressed slightly in HUVECs but was not induced by LysoPC (0.85±0.13). To confirm it, the following experiment was performed. Because LAT3 has been shown not to transport L-histidine or L-tryptophan,[23] a competitive experiment was performed using 1 mmol/L L-leucine, L-histidine, and L-tryptophan. The uptake of L-[^{14}C]leucine induced by LysoPC was competitively inhibited by these amino acids. These results suggest that the increase in L-[^{14}C]leucine uptake induced by LysoPC was attributable to pronounced LAT1 activation.

Contribution of *SLC3A2* and *SLC7A5* Expression to Cytokine Production in HUVECs

It has been reported that LAT1 is upregulated in malignant tumors, and its expression is related to the growth and proliferation of tumor cells. Therefore, we investigated whether cell proliferation would be enhanced after exposure of HUVECs to LysoPC. An enhancement of cell proliferation by LysoPC was not observable, at least as assessed by crystal violet assay and trypan blue assay (data not shown).

To find consequences of amino acid uptake into cells, cytokines released into the culture medium were measured using a BioPlex cytokine analyzer, which has the capacity to measure 17 distinct cytokines. HUVEC exposure to 30 μmol/L LysoPC for 24 hours significantly increased the release of IL-6 and IL-8 into medium (Figure 4). Release of

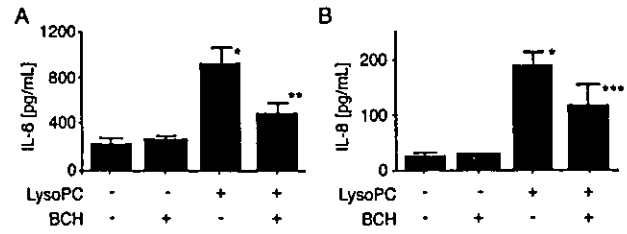

Figure 4. Cytokine release induced by LysoPC. HUVECs were incubated with 30 μmol/L LysoPC for 24 hours. The culture medium was collected, and cytokines were measured by using Bio-Plex Cytokine Assay Kit in the absence or presence of 1 mmol/L BCH. Results for IL-6 (A) and IL-8 (B) (mean±SD; n=6) are shown. *P<0.005 vs no addition; **P<0.005 vs LysoPC; ***P<0.01 vs LysoPC.

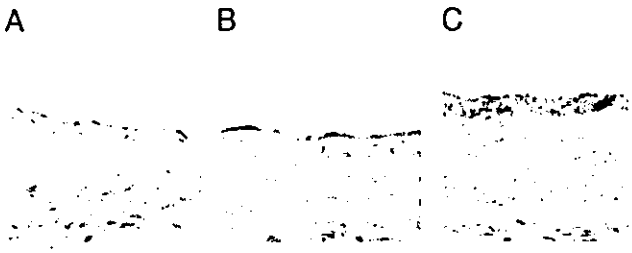

Figure 5. Detection of LAT1 in aorta of LDL receptor knockout mouse. The aortas of LDL receptor knockout mice that were fed a normal diet (A) and a high-fat diet (B) were stained by a monoclonal antibody raised against LAT1. LAT1 was expressed in endothelial cells of mice on a high-fat diet but not with a normal diet. LAT1 was also expressed in macrophages accumulating in the intima of aortas of mice fed a high-fat diet (C).

IL-6 and IL-8 from HUVECs after exposure to LysoPC was inhibited by BCH by ≈40% and 50%, respectively. BCH did not affect basal levels of IL-6 and IL-8 in the absence of LysoPC, suggesting that a substantial part of the increase in production of IL-6 and IL-8 induced by LysoPC was attributable to LAT1. IL-6 and IL-8 might also be produced using endogenous intracellular pools of amino acids in HUVECs on stimulation by LysoPC, and thus would not be inhibited by the transporter inhibitor. No release of the cytokines IL-1β, IL-2, IL-4, IL-5, IL-7, IL-10, IL-12p70, IL-13, IL-17, macrophage inflammatory protein 1-β, interferon γ (INF-γ), granulocyte-colony stimulating factor (CSF), granulocyte-macrophage CSF, tumor necrosis factor α, or monocyte chemoattractant protein 1 was detected after exposure of HUVECs to LysoPC (data not shown).

Detection of LAT1 in LDL Receptor Knockout Mouse Aorta

To test induction of LAT1 expression in atherogenic animals, immunohistochemical study using a monoclonal antibody against LAT1 was performed for aortas of LDL receptor knockout mice fed with high-fat or normal diet (Figure 5). LAT1 was detected predominantly in endothelial cells and macrophages but not smooth muscle cells in ascending aortas of mice on a high-fat diet compared with mice on a normal diet.

Discussion

OxLDL contains a variety of lipid oxidation products derived from phosphatidylcholine, CEs, fatty acids, and cholesterol. LysoPC is thought to be one of the major oxidation products of oxLDL, and its biological function in vascular cells has been investigated extensively.[13–16] A number of studies have shown that LysoPC stimulates endothelial cells to promote expression of adhesion molecules[24–26] and release cytokines.[27,28] A large-scale analysis of gene expression in HUVECs after exposure to oxLDL and lipid oxidation products including LysoPC revealed the unexpected finding that oxLDL and its components such as LysoPC affect the functions of endothelial cells by enhancing amino acid transport into cells.

SLC3A2 and *SLC7A5* are translated into the heavy chain of 4F2hc and LAT1, respectively. These proteins form a functional complex for the transport of large neutral amino acids into the cell. Because LAT1 has been shown to be expressed highly in certain cancer cell lines[18] as well as malignant

tumors,[22] its contribution to cell proliferation is strongly implicated. The enhancement of proliferation is more important in the smooth muscle cells than endothelial cells in the vascular wall but may also play a role in the balance between endothelial cell growth and apoptosis in response to injury. Because LAT1 activity regulation has become a target in cancer therapy, a specific inhibitor for LAT1 is now under active investigation. This article reports evidence for a novel function of oxLDL and its components in atherogenesis and suggests that LAT1 may prove to be a useful target molecule in inflammatory diseases.

Among the 17 cytokines measured, IL-6 and IL-8 were induced by LysoPC treatment in HUVECs. There is a binding site for C/EBPβ in the promoter region of IL-6 and IL-8.[29–33] The induction of C/EBPβ mRNA by LysoPC was examined by a GeneChip experiment (Table, fold change 6.59±2.54), and the evident genetic activity may account for a substantial part of this increased production of IL-6 and IL-8. C/EBPβ mRNA was also increased by oxLDL, 4HNE, and 22(*R*)-hydroxycholesterol. In addition, GeneChip analysis revealed that the mRNA level of IL-6 was significantly increased by LysoPC (fold change 2.35±0.35). However, a significant induction of IL-8 mRNA could not be confirmed because its basal level was too low to evaluate and allow statistical analysis. According to computer analysis of the ideal transcription factor binding sites in the promoter region, 4 C/EBPβ binding sites were found within 2000 bp in the promoter region of both *SLC3A2* and *SLC7A5*. The molecular mechanisms by which amino acid transporter gene expression is enhanced by LysoPC have yet to be elucidated, but overexpression of the transporter may account in part for the proinflammatory effects of LysoPC. It has been reported that the promoter region of *SLC3A2* displays sequence homologies with IL-2 and the IL-2 receptor α chain, the induction of which is important for T-cell activation.[34,35] In contrast to cytokines, a relationship between amino acid transport and adhesion molecule expression was not observed (see online supplement).

Computer analysis suggests that in the promoter region, there are certain other transcription factor-binding sites such as AP-1, cAMP response element-binding protein (CREB), SREBP, and specificity protein 1 (Sp1) for *SLC3A2*; and in addition to them, there is a nuclear factor κB (NF-κB) site in that of *SLC7A5*. Several signaling pathways active in endothelial cells have been identified after exposure to LysoPC. Phosphorylation of CREB by LysoPC is reported in bovine arterial endothelial cells,[36,37] and NF-κB activation has been shown to occur in response to LysoPC and prevented by protein tyrosine kinase inhibitors but not by cAMP-dependent protein kinases or PKC inhibitors.[26] However, Sugiyama et al report that NF-κB activation by LysoPC is concentration-dependent, biphasically regulated, and PKC activation might be involved in part in the LysoPC-induced NF-κB activation in HUVECs.[13] They also have shown that LysoPC increases the activities of AP-1 and CREB but not Sp1 and that only AP-1 activation in their experiments was PKC dependent. In addition to the PKC pathway, the mitogen-activated protein (MAP) kinases (ERK1/2) and the c-Jun N-terminal kinases are known to act as AP-1 activators.[13,38,39] The overexpression of dual-specificity phosphatase 1 suggests activation of MAP–kinase pathways (Table).[40] The signaling pathway crucial for the LysoPC-induced expression of *SLC3A2* and *SLC7A5* is under continuing investigation.

Acknowledgments

This work was supported in part by a grant-in-aid of Special Coordination Funds for Promoting Science and Technology from the Ministry of Education, Culture, Sports, Science and Technology. We thank Drs. Yasukazu Yoshida, Satoshi Yamada, and Koichi Sumi for helping measurements of LysoPC, HNE-adduct, and cytokines, respectively. We also thank Akashi Izumi, Akiko Kikuchi, and Chizuru Nagao for excellent technical assistance.

References

1. Steinberg D, Parthasarathy S, Carew TE, Khoo JC, Witztum JL. Beyond cholesterol. Modifications of low-density lipoprotein that increase its atherogenicity. *N Engl J Med.* 1989;320:915–924.
2. Palinski W, Rosenfeld ME, Yla-Herttuala S, Gurtner GC, Socher SS, Butler SW, Parthasarathy S, Carew TE, Steinberg D, Witztum JL. Low density lipoprotein undergoes oxidative modification in vivo. *Proc Natl Acad Sci U S A.* 1989;86:1372–1376.
3. Esterbauer H, Gebicki J, Puhl H, Jurgens G. The role of lipid peroxidation and antioxidants in oxidative modification of LDL. *Free Radical Biol Med.* 1992;13:341–390.
4. Noguchi N, Gotoh N, Niki E. Dynamics of the oxidation of low density lipoprotein induced by free radicals. *Biochim Biophys Acta.* 1993;1168:348–357.
5. Esterbauer H, Schaur RJ, Zollner H. Chemistry and biochemistry of 4-hydroxynonenal, malonaldehyde and related aldehydes. *Free Radical Biol Med.* 1991;11:81–128.
6. Uchida K, Shiraishi M, Naito Y, Torii Y, Nakamura Y, Osawa T. Activation of stress signaling pathways by the end product of lipid peroxidation. 4-hydroxy-2-nonenal is a potential inducer of intracellular peroxide production. *J Biol Chem.* 1999;274:2234–2242.
7. Dickinson DA, Iles KE, Watanabe N, Iwamoto T, Zhang H, Krzywanski DM, Forman HJ. 4-hydroxynonenal induces glutamate cysteine ligase through JNK in HBE1 cells. *Free Radical Biol Med.* 2002;33:974.
8. Cheng JZ, Singhal SS, Sharma A, Saini M, Yang Y, Awasthi S, Zimniak P, Awasthi YC. Transfection of mGSTA4 in HL-60 cells protects against 4-hydroxynonenal-induced apoptosis by inhibiting JNK-mediated signaling. *Arch Biochem Biophys.* 2001;392:197–207.
9. Camandola S, Scavazza A, Leonarduzzi G, Biasi F, Chiarpotto E, Azzi A, Poli G. Biogenic 4-hydroxy-2-nonenal activates transcription factor AP-1 but not NF-kappa B in cells of the macrophage lineage. *Biofactors.* 1997;6:173–179.
10. Hayden JM, Brachova L, Higgins K, Obermiller L, Sevanian A, Khandrika S, Reaven PD. Induction of monocyte differentiation and foam cell formation in vitro by 7-ketocholesterol. *J Lipid Res.* 2002;43:26–35.
11. Janowski BA, Grogan MJ, Jones SA, Wisely GB, Kliewer SA, Corey EJ, Mangelsdorf DJ. Structural requirements of ligands for the oxysterol liver X receptors LXRα and LXRβ. *Proc Natl Acad Sci U S A.* 1999;96:266–271.
12. Brown AJ, Sun L, Feramisco JD, Brown MS, Goldstein JL. Cholesterol addition to ER membranes alters conformation of SCAP, the SREBP escort protein that regulates cholesterol metabolism. *Mol Cell.* 2002;10:237–245.
13. Sugiyama S, Kugiyama K, Ogata N, Doi H, Ota Y, Ohgushi M, Matsumura T, Oka H, Yasue H. Biphasic regulation of transcription factor nuclear factor-kappaB activity in human endothelial cells by lysophosphatidylcholine through protein kinase C-mediated pathway. *Arterioscler Thromb Vasc Biol.* 1998;18:568–576.
14. Motley ED, Kabir SM, Gardner CD, Eguchi K, Frank GD, Kuroki T, Ohba M, Yamakawa T, Eguchi S. Lysophosphatidylcholine inhibits insulin-induced Akt activation through protein kinase C-α in vascular smooth muscle cells. *Hypertension.* 2002;39:508–512.
15. Takahashi M, Okazaki H, Ogata Y, Takeuchi K, Ikeda U, Shimada K. Lysophosphatidylcholine induces apoptosis in human endothelial cells through a p38-mitogen-activated protein kinase-dependent mechanism. *Atherosclerosis.* 2002;161:387–394.
16. Yamakawa T, Tanaka S, Yamakawa Y, Kamei J, Numaguchi K, Motley ED, Inagami T, Eguchi S. Lysophosphatidylcholine activates extracellular signal-regulated kinases 1/2 through reactive oxygen species in rat vascular smooth muscle cells. *Arterioscler Thromb Vasc Biol.* 2002;22:752–758.
17. Christensen HN. Role of amino acid transport and countertransport in nutrition and metabolism. *Physiol Rev.* 1990;70:43–77.

18. Kanai Y, Segawa H, Miyamoto K, Uchino H, Takeda E, Endou H. Expression cloning and characterization of a transporter for large neutral amino acids activated by the heavy chain of 4F2 antigen (CD98). *J Biol Chem.* 1998;273: 23629–23632.
19. Nakamura E, Sato M, Yang H, Miyagawa F, Harasaki M, Tomita K, Matsuoka S, Noma A, Iwai K, Minato N. 4F2 (CD98) heavy chain is associated covalently with an amino acid transporter and controls intracellular trafficking and membrane topology of 4F2 heterodimer. *J Biol Chem.* 1999;274:3009–3016.
20. Prasad PD, Wang H, Huang W, Kekuda R, Rajan DP, Leibach FH, Ganapathy V. Human LAT1, a subunit of system L amino acid transporter: molecular cloning and transport function. *Biochem Biophys Res Commun.* 1999;255: 283–288.
21. Yanagida O, Kanai Y, Chairoungdua A, Kim DK, Segawa H, Nii T, Cha SH, Matsuo H, Fukushima J, Fukasawa Y, Tani Y, Taketani Y, Uchino H, Kim JY, Inatomi J, Okayasu I, Miyamoto K, Takeda E, Goya T, Endou H. Human L-type amino acid transporter 1 (LAT1): characterization of function and expression in tumor cell lines. *Biochim Biophys Acta.* 2001;1514:291–302.
22. Wolf DA, Wang S, Panzica MA, Bassily NH, Thompson NL. Expression of a highly conserved oncofetal gene, TA1/E16, in human colon carcinoma and other primary cancers: homology to *Schistosoma mansoni* amino acid permease and *Caenorhabditis elegans* gene products. *Cancer Res.* 1996;56:5012–5022.
23. Babu E, Kanai Y, Chairoungdua A, Kim do K, Iribe Y, Tangtrongsup S, Jutabha P, Li Y, Ahmed N, Sakamoto S, Anzai N, Nagamori S, Endou H. Identification of a novel system L amino acid transporter structurally distinct from heterodimeric amino acid transporters. *J Biol Chem.* 2003;278:43838–43845.
24. Kume N, Cybulsky MI, Gimbrone MA Jr. Lysophosphatidylcholine, a component of atherogenic lipoproteins, induces mononuclear leukocyte adhesion molecules in cultured human and rabbit arterial endothelial cells. *J Clin Invest.* 1992;90:1138–1144.
25. Murohara T, Scalia R, Lefer AM. Lysophosphatidylcholine promotes P-selectin expression in platelets and endothelial cells. Possible involvement of protein kinase C activation and its inhibition by nitric oxide donors. *Circ Res.* 1996;78: 780–789.
26. Zhu Y, Lin JH, Liao HL, Verna L, Stemerman MB. Activation of ICAM-1 promoter by lysophosphatidylcholine: possible involvement of protein tyrosine kinases. *Biochim Biophys Acta.* 1997;1345:93–98.
27. Liu-Wu Y, Hurt-Camejo E, Wiklund O. Lysophosphatidylcholine induces the production of IL-1β by human monocytes. *Atherosclerosis.* 1998;137:351–357.
28. Rong JX, Berman JW, Taubman MB, Fisher EA. Lysophosphatidylcholine stimulates monocyte chemoattractant protein-1 gene expression in rat aortic smooth muscle cells. *Arterioscler Thromb Vasc Biol.* 2002;22:1617–1623.
29. Akira S, Isshiki H, Sugita T, Tanabe O, Kinoshita S, Nishio Y, Nakajima T, Hirano T, Kishimoto T. A nuclear factor for IL-6 expression (NF-IL6) is a member of a C/EBP family. *EMBO J.* 1990;9:1897–1906.
30. Kinoshita S, Akira S, Kishimoto T. A member of the C/EBP family, NF-IL6 β forms a heterodimer and transcriptionally synergizes with NF-IL6. *Proc Natl Acad Sci USA.* 1992;89:1473–1476.
31. Poli V. The role of C/EBP isoforms in the control of inflammatory and native immunity functions. *J Biol Chem.* 1998;273:29279–29282.
32. Kumar A, Knox AJ, Boriek AM. CCAAT/enhancer-binding protein and activator protein-1 transcription factors regulate the expression of interleukin-8 through the mitogen-activated protein kinase pathways in response to mechanical stretch of human airway smooth muscle cells. *J Biol Chem.* 2003;278:18868–18876.
33. Roux P, Alfieri C, Hrimech M, Cohen EA, Tanner JE. Activation of transcription factors NF-kappaB and NF-IL-6 by human immunodeficiency virus type 1 protein R (Vpr) induces interleukin-8 expression. *J Virol.* 2000;74:4658–4665.
34. Gottesdiener KM, Karpinski BA, Lindsten T, Strominger JL, Jones NH, Thompson CB, Leiden JM. Isolation and structural characterization of the human 4F2 heavy-chain gene, an inducible gene involved in T-lymphocyte activation. *Mol Cell Biol.* 1988;8:3809–3819.
35. Lindsten T, June CH, Thompson CB, Leiden JM. Regulation of 4F2 heavy-chain gene expression during normal human T-cell activation can be mediated by multiple distinct molecular mechanisms. *Mol Cell Biol.* 1988;8:3820–3826.
36. Ueno Y, Kume N, Miyamoto S, Morimoto M, Kataoka H, Ochi H, Nishi E, Moriwaki H, Minami M, Hashimoto N, Kita T. Lysophosphatidylcholine phosphorylates CREB and activates the jun2TRE site of c-jun promoter in vascular endothelial cells. *FEBS Lett.* 1999;457:241–245.
37. Rikitake Y, Hirata K, Kawashima S, Takeuchi S, Shimokawa Y, Kojima Y, Inoue N, Yokoyama M. Signaling mechanism underlying COX-2 induction by lysophosphatidylcholine. *Biochem Biophys Res Commun.* 2001;281:1291–1297.
38. Cieslik K, Zembowicz A, Tang JL, Wu KK. Transcriptional regulation of endothelial nitric-oxide synthase by lysophosphatidylcholine. *J Biol Chem.* 1998;273: 14885–14890.
39. Fang X, Gibson S, Flowers M, Furui T, Bast RC Jr, Mills GB. Lysophosphatidylcholine stimulates activator protein 1 and the c-Jun N-terminal kinase activity. *J Biol Chem.* 1997;272:13683–13689.
40. Haneda M, Sugimoto T, Kikkawa R. Mitogen-activated protein kinase phosphatase: a negative regulator of the mitogen-activated protein kinase cascade. *Eur J Pharmacol.* 1999;365:1–7.

nature genetics

Mutations in *SLC6A19*, encoding B^0AT1, cause Hartnup disorder

Robert Kleta[1,2], Elisa Romeo[3], Zorica Ristic[3], Toshihiro Ohura[4], Caroline Stuart[1], Mauricio Arcos-Burgos[1], Mital H Dave[3], Carsten A Wagner[3], Simone R M Camargo[3], Sumiko Inoue[5], Norio Matsuura[5], Amanda Helip-Wooley[1], Detlef Bockenhauer[6], Richard Warth[7], Isa Bernardini[1], Gepke Visser[8], Thomas Eggermann[9], Philip Lee[10], Arthit Chairoungdua[11], Promsuk Jutabha[11], Ellappan Babu[11], Sirinun Nilwarangkoon[11], Naohiko Anzai[11], Yoshikatsu Kanai[11,12], Francois Verrey[3,12], William A Gahl[1,2,12] & Akio Koizumi[5,12]

Hartnup disorder, an autosomal recessive defect named after an English family described in 1956 (ref. 1), results from impaired transport of neutral amino acids across epithelial cells in renal proximal tubules and intestinal mucosa. Symptoms include transient manifestations of pellagra (rashes), cerebellar ataxia and psychosis[1,2]. Using homozygosity mapping in the original family in whom Hartnup disorder was discovered, we confirmed that the critical region for one causative gene was located on chromosome 5p15 (ref. 3). This region is homologous to the area of mouse chromosome 13 that encodes the sodium-dependent amino acid transporter B^0AT1 (ref. 4). We isolated the human homolog of B^0AT1, called *SLC6A19*, and determined its size and molecular organization. We then identified mutations in *SLC6A19* in members of the original family in whom Hartnup disorder was discovered and of three Japanese families. The protein product of *SLC6A19*, the Hartnup transporter, is expressed primarily in intestine and renal proximal tubule and functions as a neutral amino acid transporter.

Despite molecular characterization of other proximal tubule transporters, the neutral amino acid carrier defective in Hartnup disorder (OMIM 2345000) has resisted genetic identification[2]. We carried out homozygosity mapping and fine mapping in ten members of two consanguineous families (the siblings in whom Hartnup disorder was originally discovered[1]; family A; Fig. 1a) and in siblings from the US[5] (family B; Fig. 1a). We found linkage of Hartnup disorder to 5p15 only in family A, with a maximum combined multipoint lod score of 2.31 at 11.24 cM ($P = 0.01$). This confirmed our previous results showing linkage to chromosome 5p15 (ref. 3). In family B, we obtained a maximum multipoint lod score of −2.40 at 15.81 cM.

We simultaneously pursued two mouse monoamine transporter-related orphan genes, *Slc6a18* (also called *Xtrp2*; ref. 6) and *Slc6a19* (encoding B^0AT1; ref. 4). These members of the SLC6 family of transporters map to the mouse chromosomal region that is homologous to human chromosome 5p15. Both *Slc6a18* and *Slc6a19* showed abundant expression in mouse kidney, as assessed by real time RT-PCR (Fig. 2a). Immunohistochemistry confirmed expression of mouse B^0AT1 at the brush border of small intestine (data not shown) and kidney proximal tubule cells (Fig. 2b).

The human homolog, B^0AT1, is encoded by the predicted locus *SLC6A19*, with a 2,022-bp open reading frame. PCR amplification using human kidney cDNA produced a 1,905-bp product with 100% identity to *SLC6A19* sequence. We next determined the genomic organization of *SLC6A19*, which has a stop codon 28 bases before the ATG in the 5′ untranslated region. *SLC6A19* has 12 coding exons. The B^0AT1 protein contains 634 amino acids and 12 predicted transmembrane regions (Fig. 1b). In a panel of human cDNAs, we detected robust expression of *SLC6A19* in kidney and small intestine, with minimal expression in pancreas (Fig. 2c). *SLC6A19* was also expressed in stomach, liver, duodenum and ileocecum (data not shown). In contrast, human *SLC6A18* was abundantly expressed in human kidney but not in human intestine (data not shown). These findings indicated that *SLC6A19* was the primary candidate for the gene causing Hartnup disorder.

We sequenced *SLC6A19* in six families with typical neutral aminoaciduria (Fig. 1a) and identified five mutations in *SLC6A19*

[1]Medical Genetics Branch, 10 Center Drive, MSC 1851, Building 10, Room 10C-107, National Human Genome Research Institute, National Institutes of Health, Bethesda, Maryland, USA. [2]Office of Rare Diseases, Intramural Program, Office of the Director, National Institutes of Health, Bethesda, Maryland, USA. [3]Institute of Physiology, University of Zurich, Zurich, Switzerland. [4]Department of Pediatrics, Tohoku University School of Medicine, Sendai, Japan. [5]Kyoto University Graduate School of Medicine, Kyoto, Japan. [6]Department of Pediatrics, Yale University School of Medicine, New Haven, Connecticut, USA. [7]Institut fuer Physiologie der Universitaet Regensburg, Regensburg, Germany. [8]Department of Metabolic Diseases, Wilhelmina Children's Hospital, University Hospital Utrecht, Utrecht, The Nederlands. [9]Institute of Human Genetics, Aachen University Hospital, Aachen, Germany. [10]The Charles Dent Metabolic Unit, The National Hospital for Neurology and Neurosurgery, UK. [11]Department of Pharmacology and Toxicology, Kyorin University School of Medicine, Mitaka, Tokyo, Japan. [12]These authors contributed equally to this work. Correspondence should be addressed to R.K. (kletar@mail.nih.gov).

Published online 1 August 2004; doi:10.1038/ng1405

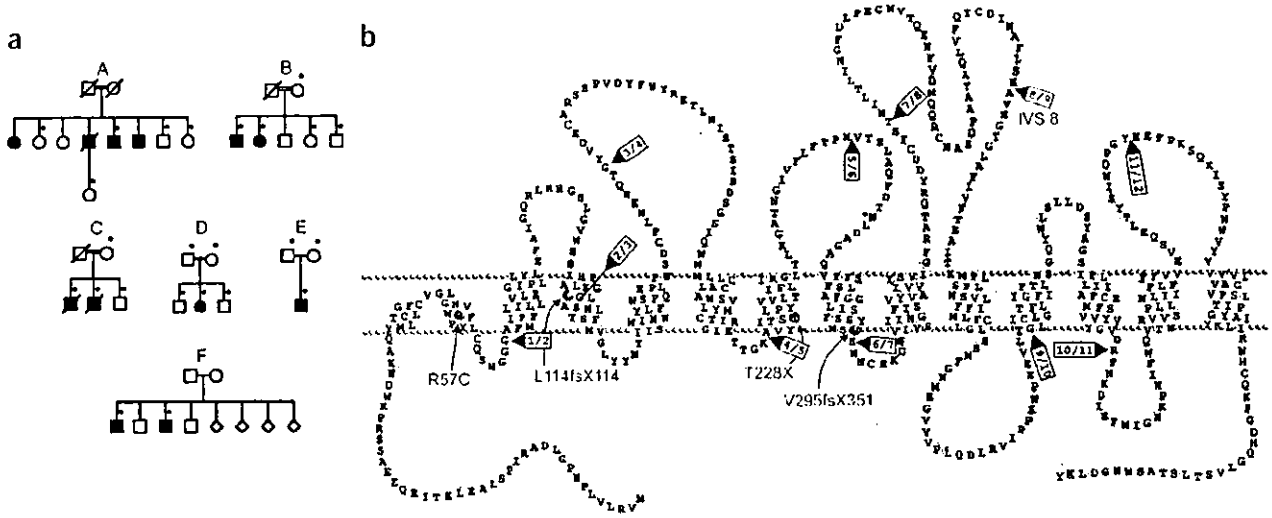

Figure 1 Families with Hartnup disorder and topology of B^0AT1 and its mutations. (a) Families with Hartnup disorder. In family A (in whom Hartnup disorder was originally discovered), a splice site mutation in *SLC6A19* segregates with Hartnup disorder. Asterisks indicate individuals from whom DNA was available for analysis. (b) Depiction of B^0AT1 in the plasma membrane. Mutations are indicated in red; arrowheads indicate splice sites.

(deletion, nonsense, missense and splice site) in four families (Table 1). Family A had a homozygous splice site mutation, IVS8+2T→G, that segregated with the phenotype. Family C (Japanese) had two affected individuals who were homozygous with respect to 884–885delTG in exon 3. A single affected member of family D (Japanese) had a homozygous missense mutation in exon 1, 169C→T, changing the conserved Arg57 to a cysteine residue. This occurred in the first membrane segment of B^0AT1 (Fig. 1b) and was not present in 100 Japanese control alleles. We identified an individual with asymptomatic Hartnup disorder in family E (Japanese; Fig. 1a) by neonatal mass screening. He was compound heterozygous with respect to c340delC in exon 2 and the nonsense mutation 682–683AC→TA in

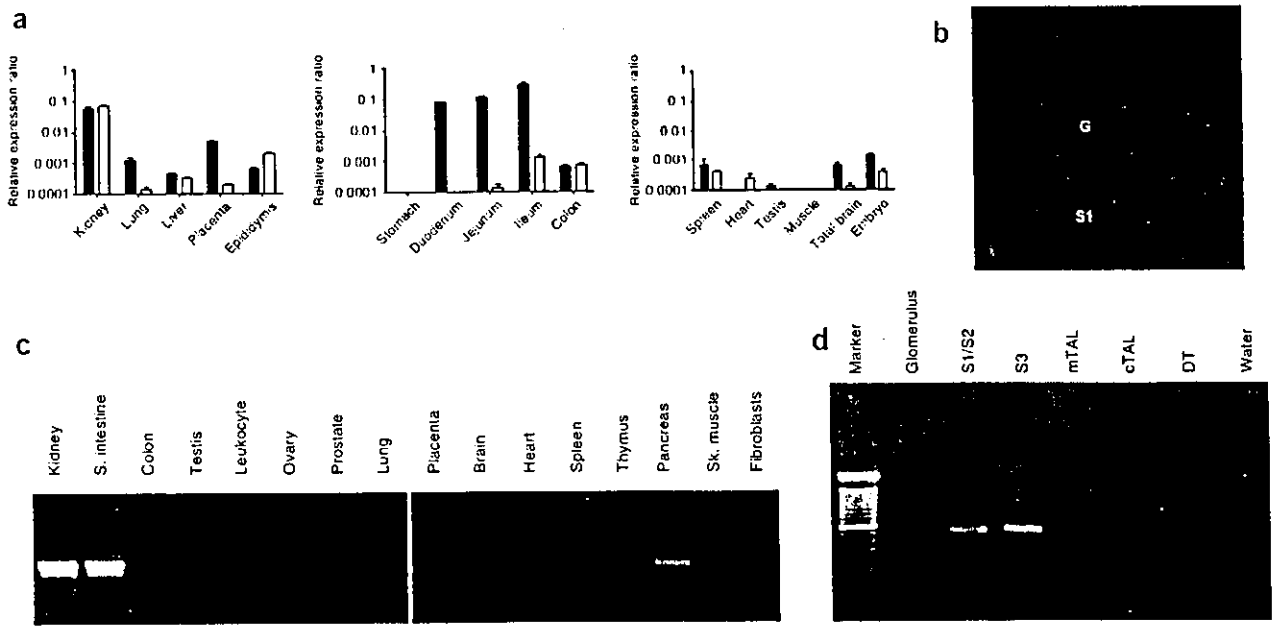

Figure 2 Expression of B^0AT1 and *Slc6a18* in mouse tissues and human tissue expression profile for the Hartnup transporter *SLC6A19* (encoding B^0AT1). (a) Relative expression ratios from real-time RT-PCR expression profiles of mouse *Slc6a19* (black bars) and mouse *Slc6a18* (gray bars). Error bars represent s.e.m. (b) Immunofluorescence of B^0AT1 (red) and of the basolateral protein 4F2hc (green) indicates the luminal expression of B^0AT1 in kidney proximal tubule (highest in segment S1). G, glomerulus. The proximal tubule cells of mouse kidney start in the glomerular capsule. (c) PCR amplification of *SLC6A19* cDNA in a panel of human tissues. *SLC6A19* was highly expressed in kidney and small intestine, and weakly expressed in pancreas. (d) *SLC6A19* cDNA was amplified from cells isolated from all segments of human proximal tubule (S1/S2 and S3), but not from the glomerulus, medullary thick ascending limb (mTAL), cortical thick ascending limb (cTAL) or distal tubule (DT).

Table 1 Mutations in *SLC6A19* associated with Hartnup disorder

mRNA	Codon	Protein	Exon	Effect on mRNA	Family	Origin	Reference
IVS8+2T→G			IVS 8	Splice site mutation	Family A	UK	1
c884–885delTG	GTG→GCA	V295fsX351	6	Deletion, premature stop	Family C	Japan	3
169C→T	CGC→TGC	R57C	1	Missense mutation	Family D	Japan	3
340delC	CTA→TAG	L114fsX114	2	Deletion, premature stop	Family E	Japan	This study
682–683AC→TA	ACG→TAG	T228X	5	Nonsense mutation	Family E	Japan	This study

exon 5, with termination at amino acid 228. Families B and F, American sibships with neutral aminoaciduria[5,7], lacked mutations in exons 1–12 of *SLC6A19* and in the gene's splice sites. This finding, and the absence of linkage to chromosome 5p15 in family B, suggests that there is locus heterogeneity. Other genes, such as those encoding a complementary transporter protein, a putative associated protein, a subunit or an efflux transporter at the basolateral side of proximal tubule cells, may be involved in transepithelial neutral amino acid transport. These possibilities have precedent in the proximal tubule transport of dibasic amino acids, which is impaired in cystinuria by defects in either subunit of the heterodimeric apical cystine transporter rBAT-$b^{0,+}$AT or, in the case of lysinuric protein intolerance, in the basolateral transporter 4F2hc-y^+LAT1 (refs. 8,9).

The cellular expression of *SLC6A19* was consistent with its putative role in plasma membrane transport. We amplified total cDNA from different portions of human renal tubules by PCR using *SLC6A19* primers. Expression was apparent in all segments of the proximal tubules, but not in the glomerulus, thick ascending limb or distal tubule (Fig. 2d). Mouse B^0AT1 transported neutral amino acids in *Xenopus laevis* oocytes; the K_m for leucine was ~0.63 mM, and transport was sodium-dependent and specific for neutral amino acids[4]. We expressed human B^0AT1 in oocytes and found sodium-dependent neutral amino acid transport with a K_m for leucine of 1.2 mM (Fig. 3a–c). Transport was abolished by the missense mutation R57C in family D (Fig. 3d).

On the basis of mapping data, tissue and cellular expression, functional studies, and mutation identification in the family in whom Hartnup disorder was originally discovered and in three other families, we conclude that B^0AT1 is the Hartnup transporter, joining the transporters in the plasma membrane that are involved in human disease[10]. Similar results and conclusions were found in Australian individuals with Hartnup disorder[11].

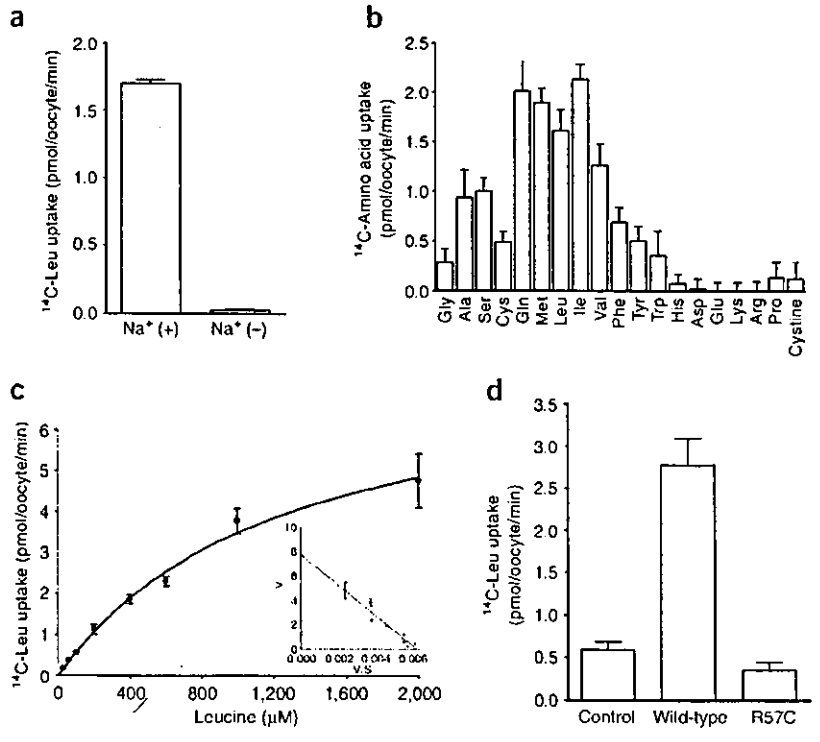

Figure 3 Function of *SLC6A19* (encoding B^0AT1). (a) B^0AT1-mediated transport of L-leucine (1 mM) was sodium-dependent. (b) The transport of ^{14}C-labeled amino acids (1 mM) mediated by *h*B^0AT1 demonstrated substrate selectivity for neutral amino acids. (c) B^0AT1-mediated transport of ^{14}C-labeled leucine was saturable and conformed to Michaelis-Menten kinetics, with K_m of 1.2 mM and V_{max} of 7.7 pmol per oocyte per min. Inset, Eadie-Hofstee plot of leucine uptake. (d) The R57C mutant of B^0AT1 (found in family D) yielded minimal uptake of ^{14}C-labeled leucine (1 mM). Error bars represent s.e.m.

METHODS

Mapping. We obtained genomic DNA from whole blood or as published previously[3] from members of families A, B, C, D and E after obtaining informed consent under a protocol approved by the National Human Genome Research Institute Institutional Review Board[3]. For family F, we extracted DNA from cells obtained from the Coriell Human Mutant Cell Repository. A genome scan using automated fluorescent microsatellite analysis of 2,011 markers, with an average marker density of 2 cM throughout the genome and an average marker heterozygosity of ~0.75, was done at deCODE Genetics. For fine mapping between *D5S1981* and *D5S464*, we used 11 polymorphic markers with an average spacing of 426 kb. We carried out linkage analyses using mapping by homozygosity with the software HOMOZ that calculates multipoint lod scores in pedigrees with inbreeding loops. We carried out two-point and multipoint parametric and nonparametric analyses of linkage using LINKAGE, with the speed improvement implemented in FASTLINK and GENEHUNTER, respectively[12–14]. We used the high-performance computational capabilities of the SGI Origin 2000 system at the Center for Information Technology of the National Institutes of Health.

Sequencing and mutation analysis. We chose intronic primers (Invitrogen) to sequence exons and splice sites of each exon. Primer sequences are available on request. We separated the PCR products of each exon by electrophoresis on agarose gels and removed specific bands for DNA isolation. We sequenced this DNA in both directions using a

Beckman Coulter CEQ8000 following the manufacturer's protocol or as published previously[3].

RNA extraction and reverse transcription. We killed male C57BL6 mice by intraperitoneal injection of ketamine and xylazine followed by cervical dislocation. We then collected tissues and rapidly froze them until further use. We collected stomach, duodenum, jejunum, ileum and colon, rinsed them several times with ice-cold phosphate buffered saline (PBS; pH 7.4), scraped off the mucosa cell layers on ice and rapidly froze them. For total RNA extraction, we thawed tissues in RLT buffer of the RNeasy Mini Kit (Qiagen) containing 10 μl ml^{-1} of β-mercaptoethanol (Sigma) and homogenized them on ice. RNA was bound to columns and treated with DNase for 15 min at 25 °C to reduce genomic DNA contamination. We used 100 ng of RNA as template for reverse transcription with TaqMan Reverse Transcription Kit (Applied Biosystems) in the presence of 2.5 μM of random hexamer primers.

Real-time PCR. We carried out real-time PCR using cDNA template and TaqMan Universal PCR master mix (Applied Biosystems). We chose primers to result in amplicons of 70–100 bp that span intron-exon boundaries. We labeled probes with reporter dye FAM at the 5′ end and the quencher dye TAMRA at the 3′ end (Microsynth). Reactions were done in 96-well optical reaction plates using a Prism 7700 cycler (Applied Biosystems). After 10 min at 95 °C, we carried out 40 cycles of 95 °C for 15 s and 60 °C for 1 min with auto-ramp time. For data analysis, we set the threshold to 0.06 (value in the linear range of amplification curves). All reactions were run in duplicate. We calculated the abundance of target mRNA relative to a reference mRNA (*GAPD*). Assuming an efficiency of 2 (relative increase in template mRNA required to decrease by 1 the number of cycles), we calculated relative expression ratios as $R = 2^{(Ct(GAPD) - Ct(test))}$, where Ct is the cycle number at the threshold and test is the tested mRNAs.

Immunohistochemistry. We anesthetized male C57BL6 mice (10–12 weeks old) with ketamine and xylazine and perfused them through the left ventricle with PBS followed by a buffered paraformaldehyde solution (4%, pH 7). We removed kidneys and small intestine, flushed them with fixative solution, cut them and embedded them in Tissue-Tek V.I.P. medium (Sakura) just before freezing in liquid nitrogen. We cut 5-μm serial sections with a cryostat and collected them on polylysine-coated slides. We incubated sections for 5 min in 0.1% SDS, washed them three times and then incubated them with the primary antibody (diluted in PBS, 0.04% Triton X-100) for 1 h at room temperature. We again washed sections three times and then incubated them with the secondary antibody (diluted in PBS, 0.04% Triton X-100) for 1 h at room temperature. After washing them five times, we mounted the sections using DAKO mounting medium and viewed them with a Leica SP1 UV CLSM confocal microscope. We used rabbit antibody to mouse B^0AT1 (antigen peptide NH_2-MVRLVLPNPGLEERIC-$CONH_2$; serum, dilution 1:200) and goat antibody to mouse 4F2hc (Santa Cruz Biotech, 1:400) as primary antibodies and donkey antibody to rabbit (1:1,000) and donkey antibody to goat (1:500; Molecular Probes) as secondary antibodies.

Segmental expression in human kidney. We carried out segment-specific dissection according to a previously described protocol[15]. We extracted total RNA and reverse transcribed it to generate segment-specific cDNA as described[16].

Functional studies. We carried out RT-PCR of *SLC6A19* cDNA (primer sequences available on request) on the first-strand cDNA generated from human kidney poly(A)$^+$ RNA (Clontech). We cloned the PCR fragment into pCR2.1-TOPO vector (Invitrogen). For the expression in oocytes, we excised the *SLC6A19* cDNA with *Eco*RI and subcloned it into pcDNA3.1(+) vector (Invitrogen). We carried out site-directed mutagenesis (R57C) of *SLC6A19* cDNA in the pcDNA3.1(+) plasmid using the QuikChange kit (Stratagene). We checked the accuracy of the cDNAs by direct sequencing. We injected *X. laevis* oocytes with 25 ng of cRNA synthesized *in vitro* from *SLC6A19* cDNA in the pcDNA3.1(+) plasmid linearized with *Not*I. We carried out *in vitro* transcription using the T7 mMESSAGE mMACHINE Kit (Ambion) and polyadenylation of the cRNA using the Poly(A) Tailing Kit (Ambion). We measured transport after 2–3 d of expression as described[17]. We measured uptake of ^{14}C-labeled amino acids in the regular uptake solution (100 mM NaCl, 2 mM KCl, 1.8 mM $CaCl_2$, 1 mM $MgCl_2$ and 5 mM HEPES buffer (pH 7.4)) or in a solution in which NaCl was replaced by choline-Cl, containing 2.5 μCi ml^{-1} of radioactively labeled compounds and 0.03–2 mM of amino acids. We measured uptake (pmol per oocyte per min) in triplicate for 30 min.

GenBank accession numbers. *SLC6A19* open reading frame, XM_291120; *SLC6A19* cDNA sequence, AY596807.

ACKNOWLEDGMENTS

We thank D. Bacic for help with frozen sections, L.G. Palacio for statistical analyses, F. Skovby for expert advice and the families who graciously participated in this study. This study was supported by Grants-in-aid from the Japanese Government to A.K. and by Swiss National Science Foundation grants to F.V.

COMPETING INTERESTS STATEMENT

The authors declare that they have no competing financial interests.

Received 20 April; accepted 17 June 2004
Published online at http://www.nature.com/naturegenetics/

1. Baron, D.N., Dent, C.E., Harris, H., Hart, E.W. & Jepson, J.B. Hereditary pellagra-like skin rash with temporary cerebellar ataxia, constant renal amino-aciduria, and other bizarre biochemical features. *Lancet* **271**, 421–428 (1956).
2. Levy, H.L. Hartnup disorder. in *The Metabolic and Molecular Bases of Inherited Disease* 8th edn., vol. III (eds. Scriver, C.R., Beaudet, A.L., Valle, D.L. & Sly, W.S.) 4957–4969 (McGraw-Hill, New York, 2001).
3. Nozaki, J. *et al.* Homozygosity mapping to chromosome 5p15 of a gene responsible for Hartnup disorder. *Biochem. Biophys. Res. Commun.* **284**, 255–260 (2001).
4. Broer, A. *et al.* Molecular cloning of mouse amino acid transport system B^0, a neutral amino acid transporter related to Hartnup disorder. *J. Biol. Chem.* **279**, 24467–24476 (2004).
5. Bernardini, I., Introne, W., Kleta, R., Fitzpatrick, D.L. & Gahl, W.A. Detection of Hartnup's disorder in an alkaptonuria sibship. *Am. J. Hum. Genet.* **69**, Suppl. 1, 1784 (2001).
6. Virkon, B. *et al.* Serial microanalysis of renal transcriptomes. *Proc. Natl. Acad. Sci. USA* **96**, 15286–15291 (1999).
7. Shih, V.E., Bixby, E.M., Alpers, D.H., Bartsocas, C.S. & Thier, S.O. Studies of intestinal transport defect in Hartnup disease. *Gastroenterology* **61**, 445–453 (1971).
8. Verrey, F. *et al.* CATs and HATs: the SLC7 family of amino acid transporters. *Pflugers Arch.* **447**, 532–542 (2004).
9. Palacin, M., Goodyer, P., Nunes, V., Gasparini & Cystinuria, P. in *The Metabolic and Molecular Bases of Inherited Disease* 8th edn., vol. III (eds. Scriver, C.R., Beaudet, A.L., Valle, D.L. & Sly, W.S.) 4909–4932 (McGraw-Hill, New York, 2001).
10. Kleta, R., Stuart, C., Gill, F.A. & Gahl, W.A. Renal glucosuria due to *SGLT2* mutations. *Mol. Genet. Metab.* **82**, 56–58 (2004).
11. Seow, H.F. *et al.* Hartnup disorder is caused by mutations in *SLC6A19*, encoding the neutral amino acid transporter. *Nat. Genet.* advance online publication, 1 August 2004 (doi:10.1038/ng1).
12. Lander, E.S. & Botstein, D. Homozygosity mapping: a way to map human recessive traits with the DNA of inbred children. *Science* **236**, 1567–1570 (1987).
13. Kruglyak, L., Daly, M.J. & Lander, E.S. Rapid multipoint linkage analysis of recessive traits in nuclear families, including homozygosity mapping. *Am. J. Hum. Genet.* **56**, 519–527 (1995).
14. Cottingham, R.W. Jr., Idury, R.M. & Schaffer, A.A. Faster sequential genetic linkage computations. *Am. J. Hum. Genet.* **53**, 252–263 (1993).
15. Schafer, J.A. *et al.* A simplified method for isolation of large numbers of defined nephron segments. *Am. J. Physiol.* **273**, F650–F657 (1997).
16. Levy, D.I., Velazques, H., Goldstein, S.A. & Bockenhauer, D. Segment-specific expression of 2P domain potassium channel genes in human nephron. *Kidney Int.* **65**, 918–926 (2004).
17. Kanai, Y. & Hediger, M.A. Primary structure and functional characterization of a high-affinity glutamate transporter. *Nature* **360**, 467–471 (1992).

ELSEVIER

Neuroscience Letters 358 (2004) 123–126

Neuroscience Letters

www.elsevier.com/locate/neulet

High affinity D- and L-serine transporter Asc-1: cloning and dendritic localization in the rat cerebral and cerebellar cortices

Hirotaka Matsuo[a,b], Yoshikatsu Kanai[b,c,*], Motohide Tokunaga[a], Takahiro Nakata[d], Arthit Chairoungdua[b], Hisako Ishimine[a], Shingo Tsukada[a], Hidetoshi Ooigawa[e], Hiroshi Nawashiro[e], Yasushi Kobayashi[d], Jun Fukuda[a], Hitoshi Endou[b]

[a] *First Department of Physiology, National Defense Medical College, 3-2 Namiki, Tokorozawa, Saitama 359-8513, Japan*
[b] *Department of Pharmacology and Toxicology, Kyorin University School of Medicine, 6-20-2 Shinkawa, Mitaka, Tokyo 181-8611, Japan*
[c] *PRESTO, Japan Science and Technology Corporation (JST), 6-20-2 Shinkawa, Mitaka, Tokyo 181-8611, Japan*
[d] *Second Department of Anatomy, National Defense Medical College, 3-2 Namiki, Tokorozawa, Saitama 359-8513, Japan*
[e] *Department of Neurosurgery, National Defense Medical College, 3-2 Namiki, Tokorozawa, Saitama 359-8513, Japan*

Received 24 December 2003; received in revised form 7 January 2004; accepted 8 January 2004

Abstract

System asc transporter Asc-1, expressed in the brain, transports D- and L-serine with high affinity. To determine the localization of Asc-1 in the rat brain, we isolated a cDNA for the rat orthologue of Asc-1. The encoded protein designated as rAsc-1 (rat Asc-1) exhibited 98% sequence identity to mouse Asc-1 (mAsc-1). Based on amino acid sequences of rAsc-1 and mAsc-1, two polyclonal antibodies against Asc-1 were generated and used for the immunohistochemical analysis on the cerebral and cerebellar cortices of rats and mice. Asc-1 immunoreactivity was detected in neurons, including cerebellar Purkinje neurons and pyramidal neurons in the neocortex and hippocampus. It was clearly localized in dendrites as well as somata. The localization of Asc-1 in brain suggests the significant contribution of Asc-1 to amino acid mobilization in brains including the synaptic clearance of D-serine and the neuronal uptake of L-serine that is essential for survival and dendrite growth of Purkinje neurons in particular.

Keywords: Amino acid transporter; System asc; Asc-1; D-Serine; L-Serine; *N*-Methyl-D-aspartate receptor; 3-Phosphoglycerate dehydrogenase; Rat

D-Serine is present in mammalian brain at high concentration [5] and known as an endogenous modulator of *N*-methyl-D-aspartate (NMDA) receptors [16]. L-Serine, the precursor of D-serine, is also important for the survival and development of neurons, especially for cerebellar Purkinje neurons because they lack L-serine biosynthetic enzyme, 3-phosphoglycerate dehydrogenase (3PGDH) [4].

We have recently identified a high affinity D- and L-serine transporter from mouse and human brain, designated as mAsc-1 (mouse Asc-1) [3,8] and hAsc-1 (human Asc-1) [12]. Asc-1 belongs to the heterodimeric amino acid transporter family [15] which associates with type II membrane glycoproteins such as 4F2 heavy chain (4F2hc) [3,11]. When co-expressed with 4F2hc, Asc-1 transports D- and L-serine at high affinity with a K_m value close to the physiological D-serine concentration [3,12]. Asc-1 is thus proposed to play significant roles in the mobilization of these amino acids. Recently, Helboe et al. reported that Asc-1 was localized in neurons, especially in presynaptic terminals in rodent brains [6]. Although neuronal localization of Asc-1 was consistent, its subcellular localization was quite different from our previous observation [9], in which Asc-1 was clearly localized on dendrites. To address this discrepancy and to determine the precise localization of Asc-1 in the rat cerebral and cerebellar cortices, we cloned a cDNA for rat orthologue of Asc-1. Based on the amino acid sequences, we generated two antibodies against Asc-1 to perform immunohistochemical analysis on rat and mouse brains.

To isolate a cDNA for rat Asc-1 (rAsc-1), a cDNA library was constructed from rat brain poly(A)$^+$RNA and screened as described [3,12]. A ^{32}P-labeled ~0.8 kb *Nco* I fragment of mAsc-1 cDNA was used as a probe.

An isolated cDNA clone with a 1938 bp insert contained an open reading frame from nucleotides 54 to 1646 encoding a putative 530 amino acid protein designated as

* Corresponding author. Department of Pharmacology and Toxicology, Kyorin University School of Medicine, 6-20-2 Shinkawa, Mitaka, Tokyo 181-8611, Japan. Tel.: +81-422-47-5511, ext. 3453; fax: +81-422-79-1321.
E-mail address: ykanai@kyorin-u.ac.jp (Y. Kanai).

0304-3940/03/$ - see front matter © 2004 Elsevier Ireland Ltd. All rights reserved.
doi:10.1016/j.neulet.2004.01.014

rAsc-1. The rAsc-1 amino acid sequence exhibited remarkable identity to those of mAsc-1 (98%) and hAsc-1 (91%) (Fig. 1). Based on the SOSUI algorithm, 12 transmembrane regions were predicted [12]. There is a conserved cysteine residue (Fig. 1) which is supposed to link to 4F2hc [15]. Consistent with mAsc-1 [3,8] and hAsc-1 [12], rAsc-1 was functional when co-expressed with rat 4F2hc in *Xenopus* oocytes (data not shown).

C-Terminal-directed polyclonal antibody was generated in rabbits [10,11] against the synthetic peptide [QGSLEEEENGPC] (amino acids 503–513 of rAsc-1). Amino acid sequences are conserved between rAsc-1 and mAsc-1 for the region of this peptide (Fig. 1). N-Terminal-directed polyclonal antibody was also generated against the peptide [RRDSDMASHIQQPC] (amino acids 2–14 of mAsc-1). In this region, only two amino acids are altered (Thr 8 and Gly 9 for rAsc-1 vs. Ala 8 and Ser 9 for mAsc-1) (Fig. 1). C-Terminal cysteine residues were used for conjugation with keyhole limpet hemocyanin. Antisera were affinity-purified as described [1]. We hereafter refer to these antibodies as anti-C-Asc-1 and anti-N-Asc-1 antibodies.

The brain tissue was obtained from adult male Sprague–Dawley rats weighing 270–320 g and adult male ICR mice weighing 30–35 g. Paraffin sections (5 μm) of the tissue were processed for immunohistochemical analysis as described previously [1,10,11]. The sections were incubated with affinity-purified anti-C-Asc-1 (1:10) or anti-N-Asc-1 antibody (1:50) overnight at 4 °C [9]. Thereafter, they were treated with Envision (+) rabbit peroxidase (DAKO) for 30 min, and colored by diaminobenzidine [9–11]. For absorption experiments, the sections were treated with the primary antibodies in the presence of antigen peptides (50 μg/ml) [10,11].

Immunohistochemical analysis on the rat cerebral cortex with anti-C-Asc-1 antibody showed intense Asc-1 immunoreactivity (Asc-1-ir) in pyramidal neurons in the neocortical layers III and V (Fig. 2A). Asc-1-ir in pyramidal neurons was detected in somata and dendrites, especially in the proximal portion of apical dendrites (arrowheads in Fig. 2C). In the absorption experiments, Asc-1-ir with anti-C-Asc-1 antibody was diminished (Fig. 2E), confirming the specificity of the immunoreactions. Asc-1-ir with anti-N-Asc-1 antibody revealed similar immunostaining (Fig. 2B, D,F). In the rat hippocampus, both antibodies also darkly labeled dendrites of hippocampal pyramidal neurons (Fig. 2G,H), although their somata were faintly stained. Results from the mouse hippocampus (Fig. 2I,J) and neocortex (data not shown) were consistent with those from rats.

In the immunohistochemical analysis on the rat cerebellar cortex, anti-C-Asc-1 antibody intensely labeled Purkinje neurons (Fig. 3A), especially their dendrites as well as somata (Fig. 3C). In addition, the molecular layer was faintly and diffusely labeled (Fig. 3C), as reported by Helboe et al. [6]. Similar results were obtained from rats (Fig. 3B,E) and mice (Fig. 3G) with anti-N-Asc-1 antibody. Although the immunostaining in Purkinje neurons disappeared in the absorption experiments, the diffuse staining of the molecular layer was not diminished, suggesting that the molecular layer staining is non-specific (Fig. 3D,F,H).

We also performed immunohistochemical analysis using another C-terminal-directed antibody (anti-C2-Asc-1 antibody) against the peptide [PSPLPITDKPLKTQC] (amino acids 517–530 of mAsc-1 and rAsc-1) [3] which was used by Helboe et al. [6]. However, in contrast to their report [6], we could not obtain any specific stainings in the rat cerebral and cerebellar cortices both for anti-C2-antiserum and its affinity-purified antibody (data not shown).

Using two different antibodies, anti-C-Asc-1 and anti-N-Asc-1, consistent results were obtained for Asc-1-ir. Therefore, we concluded that Asc-1 is localized in dendrites and somata of pyramidal neurons and Purkinje neurons. Helboe et al. used the antibody against the same peptide as that for anti-C2-Asc-1 antibody and reported the labeling of presynaptic terminals instead of dendrites [6]. Although the reasons for this discrepancy are unknown, there are some possible explanations. First, there might be variant proteins due to the alternative splicing at the C-terminal region, which sometimes occurs for transporter proteins [14]. Second, a part of Asc-1-ir reported by Helboe et al. using

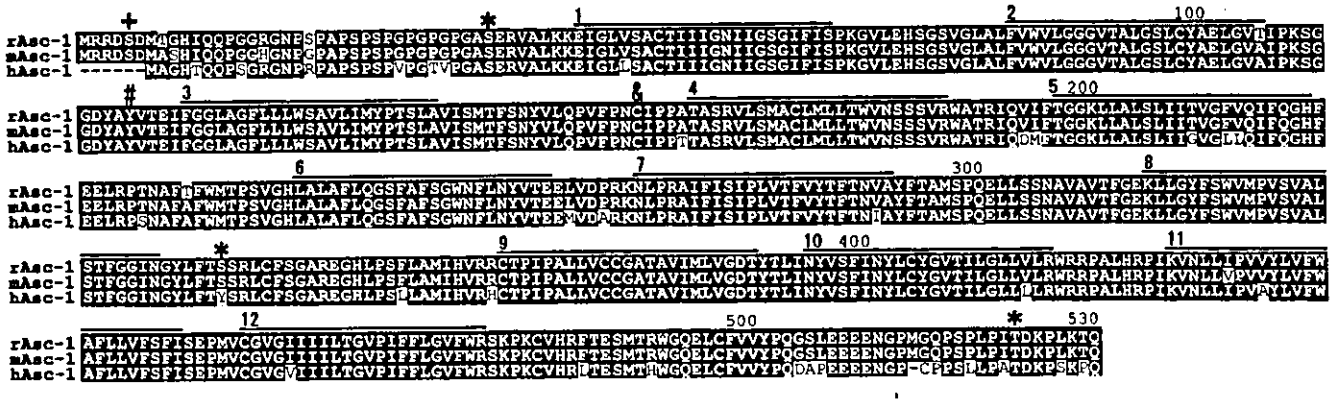

Fig. 1. Structural features of rAsc-1. The deduced sequence of rAsc-1 is aligned with those of mAsc-1 and hAsc-1. Predicted transmembrane domains are indicated by lines numbered 1–12. The conserved cysteine residue (C160) through which Asc-1 is proposed to link to 4F2hc is indicated by &. rAsc-1 has a potential tyrosine kinase-dependent phosphorylation site (#), three potential protein kinase C-dependent phosphorylation sites (*) and a potential cAMP-dependent phosphorylation site (+).

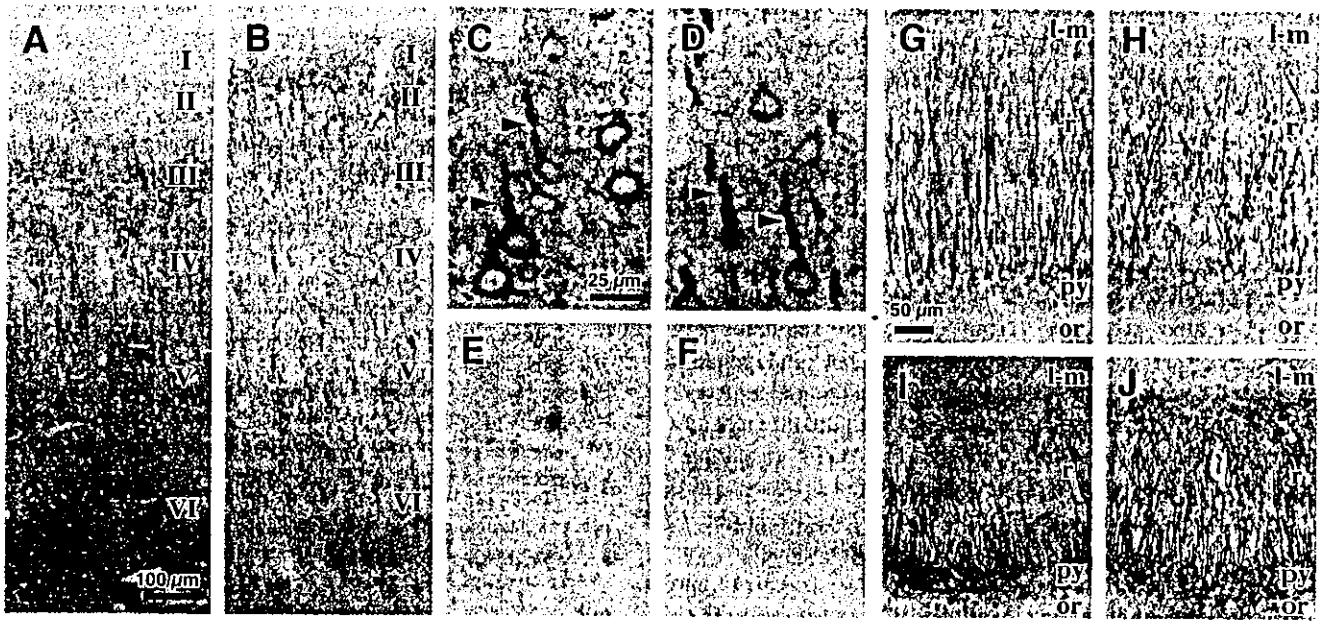

Fig. 2. Expression of Asc-1 in the cerebral cortex. Sections from rats (A–H) and mice (I,J) were stained with anti-C-Asc-1 (A,C,E,G,I) or anti-N-Asc-1 antibody (B,D,F,H,J). Asc-1 immunoreactivity (Asc-1-ir) was detected in pyramidal neurons in the cerebral neocortex (A–F) and CA1 in the hippocampus (G–J). Arrowheads in (C,D) indicate intensely labeled proximal portions of dendrites. In the absorption experiments (E,F), Asc-1-ir was diminished. Mouse brain sections (I,J) were counterstained with hematoxylin. Roman numerals, numbers of neocortical layers; l-m, stratum lacunosum-moleculare; r, stratum radiatum; py, pyramidal cell layer; or, stratum oriens. The scale in (A) applies to (A,B), the scale in (C) is for (C–F), and the scale in (G) is for (G–J).

the antiserum [6] might be less specific. The results of the absorption experiments for their antibody were not mentioned clearly by Helboe et al. [6]. Indeed, we also detected the diffuse Asc-1-ir in the molecular layer of cerebellum as Helboe et al. reported [6], however, it did not disappear in the absorption experiments.

In this study, we report the cloning of rAsc-1 and its localization in the cerebral and cerebellar cortices. Asc-1 was localized in neurons, including cerebellar Purkinje neurons and pyramidal neurons in the neocortex and hippocampus. Asc-1-ir in neurons was clearly detected in dendrites as well as somata using two different antibodies, suggesting the physiological roles of Asc-1 in neurons, such as D- and L-serine mobilization. L-Serine is shown to be essential for the survival and dendrite growth of Purkinje neurons that lack L-serine biosynthetic enzyme 3PGDH [4]. Considering the extremely low concentration of D-serine in the cerebellum (~0.5 μM) [5], it is proposed that the high affinity L-serine transporter Asc-1 in Purkinje neurons would be essential to support their survival. Moreover, obvious dendritic localization of Asc-1 implies that Asc-1-mediated L-serine uptake at dendrites could also maintain the dendrite growth of neurons such as Purkinje neurons and pyramidal neurons. Furthermore, dendritic localization of Asc-1 with high affinity to D-serine [3,12] supports the idea that Asc-1 mediates synaptic clearance of D-serine via a postsynaptic uptake mechanism.

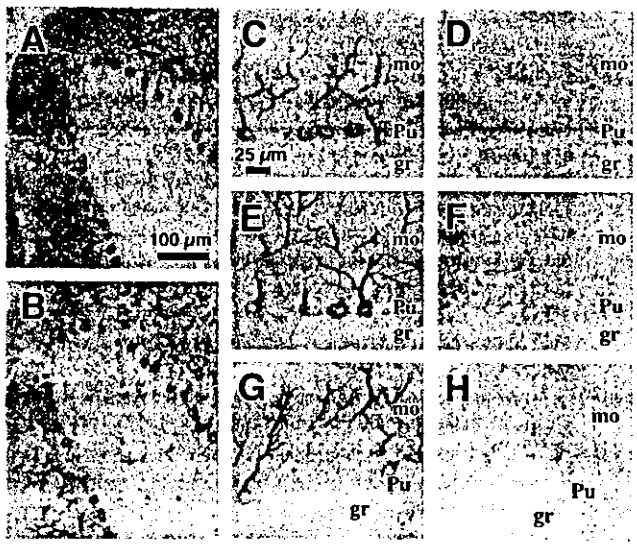

Fig. 3. Expression of Asc-1 in the cerebellar cortex. Asc-1 immunoreactivity was detected in cerebellar Purkinje neurons of rats (A–F) and mice (G,H). Sections were stained with anti-C-Asc-1 (A,C,D), or anti-N-Asc-1 antibody (B,E–H). Results from the absorption experiments are shown in (D,F,H). mo, molecular layer; Pu, Purkinje cell layer; gr, granule cell layer. The scale in (A) applies to (A,B) and the scale in (C) is for (C–H).

Prevailing evidence suggests that D-serine is involved in a variety of physiological and pathophysiological events in the brain. For example, D-serine regulates the NMDA receptor function as a co-agonist by binding to the glycine site of the receptor [16]. Recently, it has been reported that D-serine or glycine binding is also important for priming the internalization of NMDA receptors [13]. In addition, D-serine has an inhibitory effect on the excitatory glycine receptors containing the NR3 family of NMDA receptor subunits [2]. Furthermore, D-serine may be implicated to the pathophysiology of stroke and neurodegenerative disorders

involving glutamate/NMDA excitotoxicity [16] and of schizophrenia associated with NMDA receptor dysfunction [7]. D-Serine is produced by serine racemace, an enzyme in glial cells catalyzing the racemization of L-serine to D-serine. D-Serine is then released from the glial cells to the extracellular space through the transporters localized in glial plasma membrane [16]. Because Asc-1 is localized in neurons, additional D-serine transporters in glial cells are proposed to be present to mediate the D-serine release.

To search for further D-serine transporters, we analyzed Asc-1-related sequences from expressed sequence tag databases and identified an additional Na^+-independent system asc transporter. The transporter designated as Asc-2 [1] was unique because it is associated with unknown heavy chains rather than 4F2hc, similar to AGT1 (aspartate/glutamate transporter 1) structurally related to Asc-2 [10]. However, Asc-2 may not be involved in D-serine mobilization in the brain because Asc-2-mediated transport was more selective for L-serine than D-serine, just as ASCT1 and ASCT2, Na^+-dependent system ASC transporters [17]. Thus, the glial D-serine transporters still remain to be identified.

The present study on the cellular and subcellular localizations of Asc-1, together with our previous characterization of its functional properties, provides new insights into the roles of Asc-1 in the brain. Asc-1 in dendrites and somata of neurons could be involved in a variety of physiological and pathophysiological events because of the ability to transport D- and L-serine.

Acknowledgements

This work was supported in part by grants from the Ministry of Education, Culture, Sports, Science and Technology of Japan, the Japan Society for the Promotion of Science, the Promotion and Mutual Aid Corporation for Private Schools of Japan, the Japan Health Sciences Foundation (to Y.K. and H.E.), Uehara Memorial Foundation, YASUDA Medical Research Foundation (to Y.K.), Health and Labour Sciences Research Grants for Research on Advanced Medical Technology: Toxicogenomics Project (to H.E.), and Kowa Life Sciences Foundation (to H.M.). The authors also thank Michi Takahashi, Ryo Kinoshita, Akiyoshi Nakayama and Satoru Watanabe for technical assistance. Anti-Asc-1 antibodies were supplied by Kumamoto Immunochemical Laboratory, Transgenic Inc., Kumamoto, Japan. The nucleotide sequence for rAsc-1 has been submitted to the GenBank/EMBL/DDBJ Data Bank with an accession number AB126813.

References

[1] A. Chairoungdua, Y. Kanai, H. Matsuo, J. Inatomi, D.K. Kim, H. Endou, Identification and characterization of a novel member of the heterodimeric amino acid transporter family presumed to be associated with an unknown heavy chain, J. Biol. Chem. 276 (2001) 49390–49399.

[2] J.E. Chatterton, M. Awobuluyi, L.S. Premkumar, H. Takahashi, M. Talantova, Y. Shin, J. Cui, S. Tu, K.A. Sevarino, N. Nakanishi, G. Tong, S.A. Lipton, D. Zhang, Excitatory glycine receptors containing the NR3 family of NMDA receptor subunits, Nature 415 (2002) 793–798.

[3] Y. Fukasawa, H. Segawa, J.Y. Kim, A. Chairoungdua, D.K. Kim, H. Matsuo, S.H. Cha, H. Endou, Y. Kanai, Identification and characterization of a Na^+-independent neutral amino acid transporter that associates with the 4F2 heavy chain and exhibits substrate selectivity for small neutral D- and L-amino acids, J. Biol. Chem. 275 (2000) 9690–9698.

[4] S. Furuya, T. Tabata, J. Mitoma, K. Yamada, M. Yamasaki, A. Makino, T. Yamamoto, M. Watanabe, M. Kano, Y. Hirabayashi, L-Serine and glycine serve as major astroglia-derived trophic factors for cerebellar Purkinje neurons, Proc. Natl. Acad. Sci. USA 97 (2000) 11528–11533.

[5] A. Hashimoto, T. Oka, T. Nishikawa, Extracellular concentration of endogenous free D-serine in the rat brain as revealed by in vivo microdialysis, Neuroscience 66 (1995) 635–643.

[6] L. Helboe, J. Egebjerg, M. Moller, C. Thomsen, Distribution and pharmacology of alanine-serine-cysteine transporter 1 (asc-1) in rodent brain, Eur. J. Neurosci. 18 (2003) 2227–2238.

[7] D.C. Javitt, Glycine modulators in schizophrenia, Curr. Opin. Invest. Drugs 3 (2002) 1067–1072.

[8] H. Matsuo, A. Chairoungdua, D.K. Kim, S.H. Cha, J. Fukuda, H. Endou, Y. Kanai, Mouse Asc-1 (asc-type amino acid transporter 1) maps to chromosome 7, region B1-B5, Chromosome Res. 8 (2000) 456.

[9] H. Matsuo, J. Fukuda, H. Endou, Y. Kanai, Cloning, functional characterization and localization of Asc-1; A high affinity amino acid transporter for D-serine, Soc. Neurosci. Abstr. 27 (2001) 2432.

[10] H. Matsuo, Y. Kanai, J.Y. Kim, A. Chairoungdua, D.K. Kim, J. Inatomi, Y. Shigeta, H. Ishimine, S. Chaekuntode, K. Tachampa, H.W. Choi, E. Babu, J. Fukuda, H. Endou, Identification of a novel Na^+-independent acidic amino acid transporter with structural similarity to the member of a heterodimeric amino acid transporter family associated with unknown heavy chains, J. Biol. Chem. 277 (2002) 21017–21026.

[11] H. Matsuo, S. Tsukada, T. Nakata, A. Chairoungdua, D.K. Kim, S.H. Cha, J. Inatomi, H. Yorifuji, J. Fukuda, H. Endou, Y. Kanai, Expression of a system L neutral amino acid transporter at the blood-brain barrier, NeuroReport 11 (2000) 3507–3511.

[12] J. Nakauchi, H. Matsuo, D.K. Kim, A. Goto, A. Chairoungdua, S.H. Cha, J. Inatomi, Y. Shiokawa, K. Yamaguchi, I. Saito, H. Endou, Y. Kanai, Cloning and characterization of a human brain Na^+-independent transporter for small neutral amino acids that transports D-serine with high affinity, Neurosci. Lett. 287 (2000) 231–235.

[13] Y. Nong, Y.Q. Huang, W. Ju, L.V. Kalia, G. Ahmadian, Y.T. Wang, M.W. Salter, Glycine binding primes NMDA receptor internalization, Nature 422 (2003) 302–307.

[14] N. Utsunomiya-Tate, H. Endou, Y. Kanai, Tissue specific variants of glutamate transporter GLT-1, FEBS Lett. 416 (1997) 312–316.

[15] F. Verrey, E.I. Closs, C.A. Wagner, M. Palacin, H. Endou, Y. Kanai, CATs and HATs: the SLC7 family of amino acid transporters, Pflug. Arch. (2004) in press.

[16] H. Wolosker, R. Panizzutti, J. De Miranda, Neurobiology through the looking-glass: D-serine as a new glial-derived transmitter, Neurochem. Int. 41 (2002) 327–332.

[17] T. Yamamoto, I. Nishizaki, S. Furuya, Y. Hirabayashi, K. Takahashi, S. Okuyama, H. Yamamoto, Characterization of rapid and high-affinity uptake of L-serine in neurons and astrocytes in primary culture, FEBS Lett. 548 (2003) 69–73.

Reprinted from GUT, August 2004, Vol 53, No 8, p 1151-1158

COLORECTAL CANCER

Downregulation of prostaglandin E receptor subtype EP_3 during colon cancer development

Y Shoji, M Takahashi, T Kitamura, K Watanabe, T Kawamori, T Maruyama, Y Sugimoto, M Negishi, S Narumiya, T Sugimura, K Wakabayashi

Gut 2004;53:1151–1158. doi: 10.1136/gut.2003.028787

Background and aims: Involvement of prostaglandin E_2 (PGE_2) receptors EP_1, EP_2, and EP_4 in the formation of aberrant crypt foci (ACF) and/or intestinal polyps has been suggested. In contrast, EP_3 appears to have no influence on the early stages of colon carcinogenesis. In the present study, we examined expression of PGE_2 receptor subtypes EP_1, EP_2, EP_3, and EP_4 in normal colon mucosa and colon cancers, and assessed the contribution of EP_3 to colon cancer development.
Methods: mRNA expression of PGE_2 receptor subtypes EP_1, EP_2, EP_3, and EP_4 in normal colon mucosa and colon cancers in azoxymethane (AOM) treated mice and rats, and in humans, were examined by reverse transcription-polymerase chain reaction (RT-PCR), quantitative real time RT-PCR, and immunohistochemical analyses. Evaluation of the role of EP_3 was performed by intraperitoneal injection of AOM, using EP_3 receptor knockout mice. Effects of EP_3 receptor activation on cell growth of human colon cancer cell lines were examined using ONO-AE-248, an EP_3 selective agonist. Moreover, EP_3 expression in colon cancer cell lines was analysed with or without 5-aza-2′-deoxycytidine (5-aza-dC) treatment.
Results: Expression levels of EP_1 and EP_2 mRNA were increased in cancer tissues. EP_4 mRNA was constantly expressed in normal mucosa and cancers. In contrast, expression of EP_3 mRNA was markedly decreased in colon cancer tissues, being 5% in mice, 9% in rats, and 28% in humans compared with normal colon mucosa, analysed by quantitative real time RT-PCR. Immunohistochemical staining demonstrated the rat EP_3 receptor protein to be expressed in epithelial cells of normal mucosa and some parts of small carcinomas but hardly detectable in large carcinomas of the colon. Colon cancer development induced by AOM in EP_3 receptor knockout mice was enhanced compared with wild-type mice, with a higher incidence of colon tumours (78% *v* 57%) and mean number of tumours per mouse (2.17 (0.51) *v* 0.75 (0.15); $p<0.05$). Expression of EP_3 mRNA was detected in only one of 11 human colon cancer cell lines tested. Treatment with 5 μM of an EP_3 selective agonist, ONO-AE-248, resulted in a 30% decrease in viable cell numbers in the HCA-7 human colon cancer cell line in which EP_3 was expressed. Treatment with 5-aza-dC restored EP_3 expression in CACO-2, CW-2, and DLD-1 cells but not in WiDr cells, suggesting involvement of hypermethylation in the downregulation of EP_3 to some extent.
Conclusion: The PGE_2 receptor subtype EP_3 plays an important role in suppression of cell growth and its downregulation enhances colon carcinogenesis at a later stage. Hypermethylation of the EP_3 receptor gene could occur and may contribute towards downregulating EP_3 expression to some extent in colon cancers.

See end of article for authors' affiliations

Correspondence to: Dr K Wakabayashi, Cancer Prevention Basic Research Project, National Cancer Center Research Institute, 1-1, Tsukiji 5-chome, Chuo-ku, Tokyo 104-0045, Japan; kwakabay@gan2.res.ncc.go.jp

Accepted for publication 3 February 2004

Clear benefits have been reported in epidemiological studies with non-steroidal anti-inflammatory drugs (NSAIDs) as chemopreventive agents against colon cancers, one of the most common malignancies in humans.[1] Chemically induced colon carcinogenesis in rodents is also suppressed by administration of NSAIDs.[2–4] Moreover, intestinal polyp formation in familial adenomatous polyposis coli patients is markedly reduced after application of agents such as sulindac or indomethacin.[5–8] The common mechanism of action of NSAIDs is inhibition of cyclooxygenase (COX) activity, two distinct isoforms of which have been reported: a constitutive enzyme, COX-1, and an inducible enzyme, COX-2.[9] COX-1 and COX-2 are rate limiting enzymes in the synthesis of prostanoids which affect cell proliferation, tumour growth, apoptosis, and immune responsiveness, and both COX isoforms have been reported to be involved in colon carcinogenesis.[1 4 10]

Prostanoids such as prostaglandin (PG)E_2, PGD_2, $PGF_{2\alpha}$, PGI_2, and TXA_2 exert their biological actions through binding to nine specific receptors with seven transmembrane domains: the four subtypes EP_1–EP_4 for PGE_2, DP and CRTH2 for PGD_2, FP for $PGF_{2\alpha}$, IP for PGI_2, and TP for TXA_2.[11 12] Several reports have demonstrated increased levels of PGE_2 in human colon cancer tissues compared with surrounding normal mucosa.[13–15] Signal transduction pathways of PGE_2 receptors have been studied by examining agonist induced changes in the levels of second messengers such as cAMP and free Ca^{2+} and by identifying G protein coupling by various methods.[11] The EP_1 receptor is known to mediate PGE_2 induced elevation of free Ca^{2+} concentration although the species of G protein to which EP_1 receptor is coupled remains unidentified. EP_2 and EP_4 receptors are coupled to Gs and stimulate cAMP production by adenylate cyclase. In contrast, the major signalling pathway for the EP_3 receptor is inhibition of adenylate cyclase via Gi. In addition, another function has been suggested for this receptor type in which cell phenotype is regulated through activation of Rho via G proteins other than Gi.[16]

Abbreviations: PGE_2, prostaglandin E_2; ACF, aberrant crypt foci; AOM, azoxymethane; COX, cyclooxygenase; NSAIDs, non-steroidal anti-inflammatory drugs; RT-PCR, reverse transcription-polymerase chain reaction; 5-aza-dC, 5-aza-2′-deoxycytidine; FBS, fetal bovine serum

Establishment of mice lacking the genes encoding prostanoid receptors has promoted understanding of the involvement of prostanoids[11] and their receptors in the development of colon cancer.[16–18] In previous studies, we demonstrated that deficiency of either EP_1 or EP_4 receptor decreases formation of azoxymethane (AOM) induced aberrant crypt foci (ACF), putative preneoplastic lesions in the colon.[17 18] Moreover, antagonists of EP_1 and EP_4 receptors suppress formation of AOM induced ACF in the colon of mice and intestinal polyp formation in *Apc* gene deficient Min mice.[17 18] Recently, it was also reported that homozygous deletion of the gene encoding the EP_2 receptor resulted in a decrease in intestinal polyp formation in *Apc* knockout mice.[19] As already mentioned, EP_2 and EP_4 stimulate adenylate cyclase whereas EP_3 exerts an inhibitory influence, suggesting a possible suppressive role against colon carcinogenesis. However, deficiency of EP_3 did not affect AOM induced ACF formation in our previous study.[17]

In the present study, we hypothesised that EP_3 might act at a later stage in colon carcinogenesis. Examination of mRNA expression for EP_1, EP_2, EP_3, and EP_4 in colon carcinomas of mice, rats, and humans demonstrated that levels of EP_3 were markedly decreased compared with normal mucosa. An increase in colon carcinoma formation induced by AOM was also demonstrated in EP_3 receptor knockout mice. Furthermore, activation of the EP_3 receptor showed a suppressive effect on cell growth in a colon cancer cell line in which EP_3 was expressed. In most human colon cancer cell lines tested, EP_3 expression was not detected but treatment with 5-aza-2'-deoxycytidine (5-aza-dC) restored EP_3 expression in some cell lines. On the basis of the results obtained, the role of the EP_3 receptor in colon carcinogenesis is discussed.

MATERIALS AND METHODS

Animals

The mouse gene encoding the PGE_2 receptor EP_3 was disrupted by a gene knockout method using homologous recombination, as reported previously.[17] The generated chimeric mice were backcrossed with C57BL/6Cr mice, and the resulting homozygous mutant mice of these F2 progeny were backcrossed into the C57BL/6Cr background for 10 generations. EP_3 receptor deficient male mice were used at six weeks of age. Genotypes of the knockout mice were confirmed by polymerase chain reaction (PCR) according to the method described previously.[17] Animals were housed in plastic cages at 24±2℃ and 55% relative humidity with a 12 h/12 h light/dark cycle. Water and basal diet (AIN-76A; Bio-Serv, Frenchtown, New Jersey, USA) were given ad libitum. Body weights and food intake were measured weekly.

Colon tumour samples and cell lines

Mouse colon tumours and normal colon mucosa tissues were obtained from C57BL/6J male mice treated with AOM, as previously reported.[18] Rat colon tumours and normal colon mucosa tissues were obtained from eight F344 male rats treated with AOM, as previously reported.[20] Frozen samples of mouse and rat tissues were used for reverse transcription (RT)-PCR analyses, and formalin fixed, paraffin embedded rat tissue samples were employed for immunohistochemical staining.

Surgical specimens of human colon cancer and adjacent normal colon mucosa tissues were taken from eight Japanese patients who had undergone surgical operations for colorectal cancers at the National Cancer Center Hospital, Tokyo, and samples were immediately frozen in liquid nitrogen.

Eleven human colon cancer cell lines were subjected to RT-PCR analysis. HCA-7 colony 29, a human colon adenocarcinoma cell line, was kindly provided by Dr Susan Kirkland, Imperial College of Science, Technology, and Medicine (London, UK).[21] HCA-7 cells were maintained in Dulbecco's minimum essential medium supplemented with 5% heat inactivated fetal bovine serum (FBS) (Hyclone Laboratories, Inc., Logan, Utah, USA) and antibiotics (100 μg/ml of streptomycin and 100 units/ml of penicillin) at 37℃ in 5% CO_2. Colo 201, DLD-1, HCT-116, SW48, SW480, SW620, WiDr (Dainippon Pharmaceutical Co., Ltd, Osaka, Japan), CACO-2, Colo 320, and CW-2 (Riken Cell Bank, Tsukuba, Japan) were purchased and cultured according to the manufacturer's instructions.

Analysis of EP receptor expression in colon cancers by RT-PCR

Total RNA was extracted from tissues and cultured cells by direct homogenisation in Isogen (Nippon Gene Co., Tokyo, Japan), and spectrophotometry was used for quantification. Aliquots (3 μg) of total RNA were subjected to the RT reaction with oligo-dT primer using an Omniscript Reverse Transcriptase kit (Qiagen, Hilden, Germany). After reverse transcription, PCR was carried out with Hotstartaq (Qiagen), according to the manufacturer's instructions. To test cDNA integrity, the *β-actin* gene was amplified for each sample. Primers were designed using the computer program OLIGO 4.0-s (National Biosciences, Maryland, USA) and were based on published sequences in Genbank. Primers were designed to cross an exon-exon boundary or insertion of intron to ensure that genomic DNA was not being amplified. BLAST searches confirmed that the primers were specific for the target gene. Primers for the *β-actin* and *EP receptor* genes are listed in table 1. PCR amplifications were performed in a thermocycler (Gene Amp PCR System 9600; Perkin-Elmer Applied Biosystems, Foster City, California, USA), with 18–40 cycles of 94℃ for 20 seconds, 60℃ for 30 seconds, and 72℃ for one min using the specific primer sets. PCR products were then analysed by electrophoresis on 2% agarose gel.

Quantitative real time RT-PCR analysis

Quantitative real time RT-PCR analysis was performed using the Smart Cycler system with the *Ex Taq* R-PCR version 2 kit and SYBR Green (Takara Shuzo Co., Shiga, Japan) according to the manufacturer's instructions. Primers for the *β-actin* and EP_3 genes, and cycle conditions for PCR, are listed in table 2. To assess the specificity of each primer set, amplicons generated from the PCR reaction were analysed by their melting point curves and additionally run on 2% agarose gels to confirm the correct sizes of the PCR products. Each PCR product was subcloned into the TA cloning plasmid vector pGEN-T easy vector (Promega Co., Madison, Wisconsin, USA) and used as a positive control for real time PCR analyses. The number of molecules of specific gene products in each sample was determined using a standard curve generated by amplification of 10^2–10^8 copies of the control plasmid. Each sample was analysed in triplicate.

Immunohistochemical staining

Immunohistochemical analyses of colon tumours and normal mucosa samples from F344 male rats treated with AOM were performed with the avidin-biotin complex immunoperoxidase technique, as previously reported.[20] As the primary antibody, a polyclonal rabbit anti-EP_3 antibody raised against rat EP_3 receptors was used at a 50× dilution.[22] As the secondary antibody, biotinylated antirabbit IgG (H+L) raised in a goat, affinity purified, and absorbed with rat serum (Vector Laboratories, Inc., Burlingame, California, USA) was used at a 200× dilution. Staining was performed using avidin-biotin reagents (Vectastain ABC reagents; Vector Laboratories.), 3,3'-diaminobenzidine, and hydrogen